Journal of Asian Earth Sciences 115 (2016) 183–203

Contents lists available at ScienceDirect

Journal of Asian Earth Sciences

journal homepage: www.elsevier.com/locate/jseaes

A hybrid origin for two Cretaceous monzonitic plutons in eastern Zhejiang Province, Southeast China: Geochronological, geochemical, and Sr–Nd–Hf isotopic evidence

Liang Liu [a,b], Jian-Sheng Qiu [a,*], Jiao-Long Zhao [a]

[a] State Key Laboratory for Mineral Deposits Research, School of Earth Sciences and Engineering, Nanjing University, Nanjing 210023, China
[b] State Key Laboratory of Ore Deposit Geochemistry, Institute of Geochemistry, Chinese Academy of Sciences, Guiyang 550081, China

ARTICLE INFO

Article history:
Received 14 June 2015
Received in revised form 9 September 2015
Accepted 16 September 2015
Available online 18 September 2015

Keywords:
Quartz monzonites
Mafic microgranular enclaves
Geochemistry
Magma mixing
Southeast China

ABSTRACT

Monzonites can provide important information about the nature of the mantle sources and the mechanism of crust–mantle interactions. However, details on the origin of Late Mesozoic monzonites in the Southeastern China remain poorly constrained. This paper presents whole-rock geochemical, Sr–Nd isotopic and zircon U–Pb and Hf isotopic data for two monzonitic plutons (Huangtanyang and Kanggu) in eastern Zhejiang Province, with the aim of elucidating their petrogenesis, and providing important insights into the process of crust–mantle interaction. LA-ICP-MS zircon U–Pb dating results imply that the Huangtanyang and Kanggu quartz monzonites were emplaced in Cretaceous (104–109 Ma). All quartz monzonites are intermediate to acidic, metaluminous to weakly peraluminous, subalkaline, and K-rich in composition. They are enriched in large ion lithophile (e.g., Rb, Ba and Pb) and light rare earth elements, depleted in high-field strength elements (e.g., Nb, Ta, and Ti), and show weakly negative or no Eu anomalies (δEu = 0.78–1.02). All quartz monzonites have homogeneous initial I_{Sr} values (0.7084–0.7090) and $\varepsilon_{Nd}(t)$ values (−7.50 to −6.84). They are characterised by highly variable zircon Hf isotopic compositions, with $\varepsilon_{Hf}(t)$ values ranging from −13.3 to −5.7. The combined geochemical evidences (such as high Mg# values, low Nb/U and Ta/U ratios, and variable zircon Hf isotopic compositions) suggests that both depleted asthenospheric and metasomatically enriched mantle components were involved in the formation of the monzonites. The existence of some zircons with unusually low $\varepsilon_{Hf}(t)$ values (low to −13.3) and Palaeoproterozoic two-stage Hf model ages from the Huangtanyang and Kanggu quartz monzonites also argues strongly for Palaeoproterozoic crustal involvement. Magma mixing played a dominated role in the genesis of these monzonites, as indicated by their wide range in zircon Hf isotopic compositions and the occurrence of mafic microgranular enclaves (MMEs). The MMEs show spheroidal to ellipsoidal–ovoidal shapes, and have igneous mineral assemblages and disequilibrium textures, such as acicular apatite and plagioclase with complex oscillatory zoning and repeated resorption surfaces, which indicate mingling/mixing of two different magmas. MMEs from Kanggu pluton have obviously similar trace element and Sr–Nd isotopic compositions to those of the host monzonites, with I_{Sr} values of 0.7089 and $\varepsilon_{Nd}(t)$ values of −7.16, however, they are distinct in having relatively enriched Sr and P, more depleted Zr and Hf, and having relatively depleted zircon Hf isotopic compositions with $\varepsilon_{Hf}(t)$ values varying from −8.4 to −3.8. We interpret that the Huangtanyang and Kanggu plutons have a mixed origin, i.e. partial melting of crustal materials triggered by upwelling of mantle-derived magma (including depleted asthenosphere and subduction-enriched mantle, represented by MMEs) under an extensional regime, and subsequent mixing of the mantle- and crust-derived melts resulted in the monzonites.

1. Introduction

The South China Block, located on the western Pacific margin, is surrounded by the Qingling-Dabie orogenic belt to the north, the Tibetan Block to the west, and the Indochina Block to the south. The Late Mesozoic geology of Southeastern (SE) China is characterised by intensive and widespread magmatism (Fig. 1). Among the igneous rocks formed, granites and rhyolites are volumetrically predominant, with subordinate basalts and rare intermediate lithologies (Fig. 1b; Zhou et al., 2006). These igneous rocks comprise two main age groups that are of Jurassic (referred to as "Early Yanshanian" in the Chinese literature) and Cretaceous

* Corresponding author.
E-mail addresses: liuliang0830@126.com (L. Liu), jsqiu@nju.edu.cn (J.-S. Qiu), jlz2007@yeah.net (J.-L. Zhao).

http://dx.doi.org/10.1016/j.jseaes.2015.09.022
1367-9120/

("Late Yanshanian") age (Li, 2000; Zhou and Li, 2000; X.H. Li et al., 2007). Previous studies have provided considerable petrological, geochemical, and isotopic constraints on the origins and evolution of these silicic volcanic rocks (e.g., Zhou et al., 2006; Guo et al., 2012; L. Liu et al., 2012, 2014a) and, in particular, the widespread granite rocks (e.g., Griffin et al., 2002; Zhou et al., 2006; Qiu et al., 1999, 2008, 2012; Z. Li et al., 2012; Q. Liu et al., 2012). Most studies have concluded that Late Mesozoic magmatism in SE China was triggered by subduction of the palaeo-Pacific plate beneath the Eurasian plate (Jahn et al., 1990; Zhou et al., 2006; X.H. Li et al., 2007; Chen et al., 2008). However, the Late Mesozoic tectono-magmatic evolution of the SE China is still a subject of considerable controversy, especially the nature of magma sources and the crust–mantle interaction mechanism remain poor constrained (Li and Jiang, 2014a).

Monzonites commonly belong to subalkaline rocks, and are sometimes ascribed to potassic calc-alkaline series, with specific characteristics transitional between those of the calc-alkaline and alkaline rocks (Pagel and Leterrier, 1980; Pupin, 1980; Debon and Le Fort, 1983; Castro et al., 2013; Wu et al., 2014). Apart from widespread Late Mesozoic granitic rocks, there are also some small-scale monzonitic stocks developed in SE China. Some studies have examined these monzonitic stocks in recent decades, and two main different models were proposed for their origins, i.e., the first suggested that they were formed via fractional crystallisation of subduction-related enriched mantle source (Li and Jiang, 2014b), and the second advocated that the monzonites were likely generated by mixing between depleted mantle-derived mafic magmas and silicic magmas that originated from partial melting of crustal materials (Liu et al., 2013). These monzonitic stocks can thus provide important information about the nature of the mantle sources and the mechanism of crust–mantle interactions in SE China. However, the generation and geodynamic setting of most monzonitic plutons from eastern Zhejiang Province are still poor constrained.

To better understand the origins of Late Mesozoic magmatism in SE China and, in particular, the petrogenesis of monzonitic rocks, two typical monzonitic plutons, i.e., the Huangtanyang (HTY) and the Kanggu (KG) plutons in eastern Zhejiang Province, SE China were selected as examples for case studies in this paper. Our study involved a field-based investigation, followed by petrographic, geochemical, zircon U–Pb dating and Hf isotope, and whole-rock Sr–Nd isotope analyses for both monzonites and their enclaves. We use these data to constrain the nature of crustal and mantle components involved in the petrogenesis of the monzonites. More generally, these data offer new insights into the deep processes of interaction between crustal- and mantle-derived magmas beneath SE China.

2. Geological background and petrography

The South China Block (SCB) consists of the Yangtze Block to the northwest and the Cathaysia Block to the southeast (Fig. 1b). The Jiangshan-Shaoxing Fault is thought to be the boundary between the two blocks in eastern South China (Z.J. Zhang et al., 2005; Shu et al., 2008), but the southwestern extension of this boundary is unclear due to poor exposure and multiple intense tectonic modifications (X.H. Li et al., 2012). Amalgamation between the Yangtze and the Cathaysia Blocks took place in the early Neoproterozoic (e.g., Ye et al., 2007; Z.X. Li et al., 2007; Li et al., 2009). In the Triassic, the South China Block collided with the North China Block in the north, and with the Indochina Block in the southwest (Zheng et al., 2013). The unified South China Block subsequently underwent at least three major tectono-thermal events, during the early–middle Paleozoic (traditionally named as "Caledonian"), the Triassic (Indosinian) and the Jurassic–Cretaceous (Yanshanian), respectively. An abundance of igneous rocks, especially granites, formed in response to these events, with the granites in the eastern SCB commonly regarded as a large granite province (Wang and

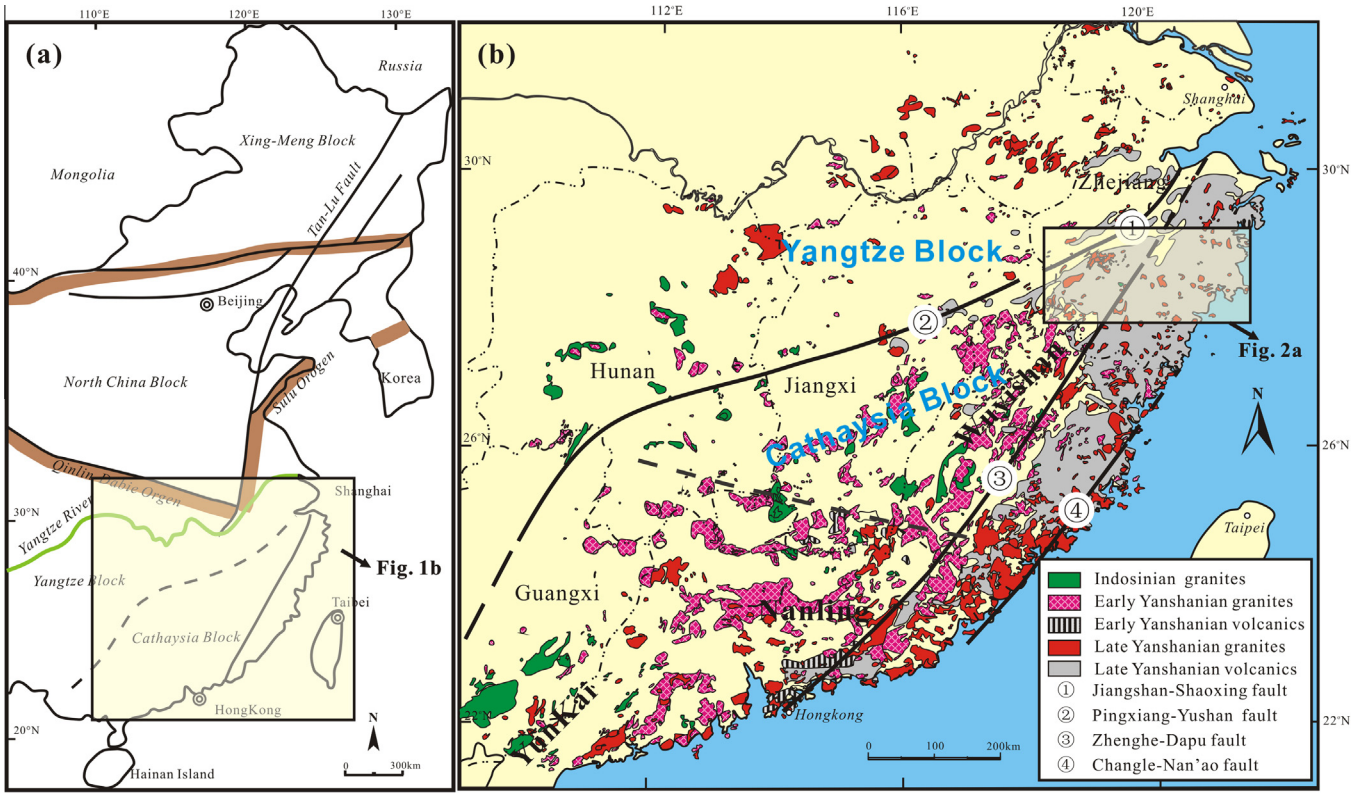

Fig. 1. (a) Simplified geological map of eastern China (modified after Li and Jiang, 2014a). (b) Simplified geological map of South China showing the distribution of Mesozoic granitoids and volcanic rocks (modified after Zhou et al., 2006).

Zhou, 2005). Late Mesozoic magmatism was largely concentrated in the Cathaysia Block, and the intensity of magmatism increased toward the ocean (Fig. 1b) (Zhou et al., 2006). Associated granitoids with Early Yanshanian (Jurassic) ages are mainly distributed in the inland region, whereas those with Late Yanshanian (Cretaceous) ages are concentrated in the coastal region. Volcanic rocks were erupted mainly in the Cretaceous and generally crop out along the coast (Zhou et al., 2006). Previous studies on the Cathaysia Block have suggested different crustal evolution histories for this block on the two sides of the Zhenghe–Dapu Fault, and therefore, this block can been further divided into two regions (the Interior or Western Cathaysia and the Coastal or Eastern Cathaysia, Chen and Jahn, 1998; Xu et al., 2007).

The Huangtanyang pluton is located in the eastern Cathaysia Block and exposed at northeastern part of Linhai County, Zhejiang Province. The pluton has a total outcrop area of ca. 13.6 km^2, and intruded into Lower Cretaceous volcanic or hypabyssal intrusive rocks of the Moshishan Group (Fig. 2b). The Huangtanyang pluton is composed mainly of quartz monzonites, and minor quartz diorites, monzogranites, and alkali-feldspar granite. The quartz

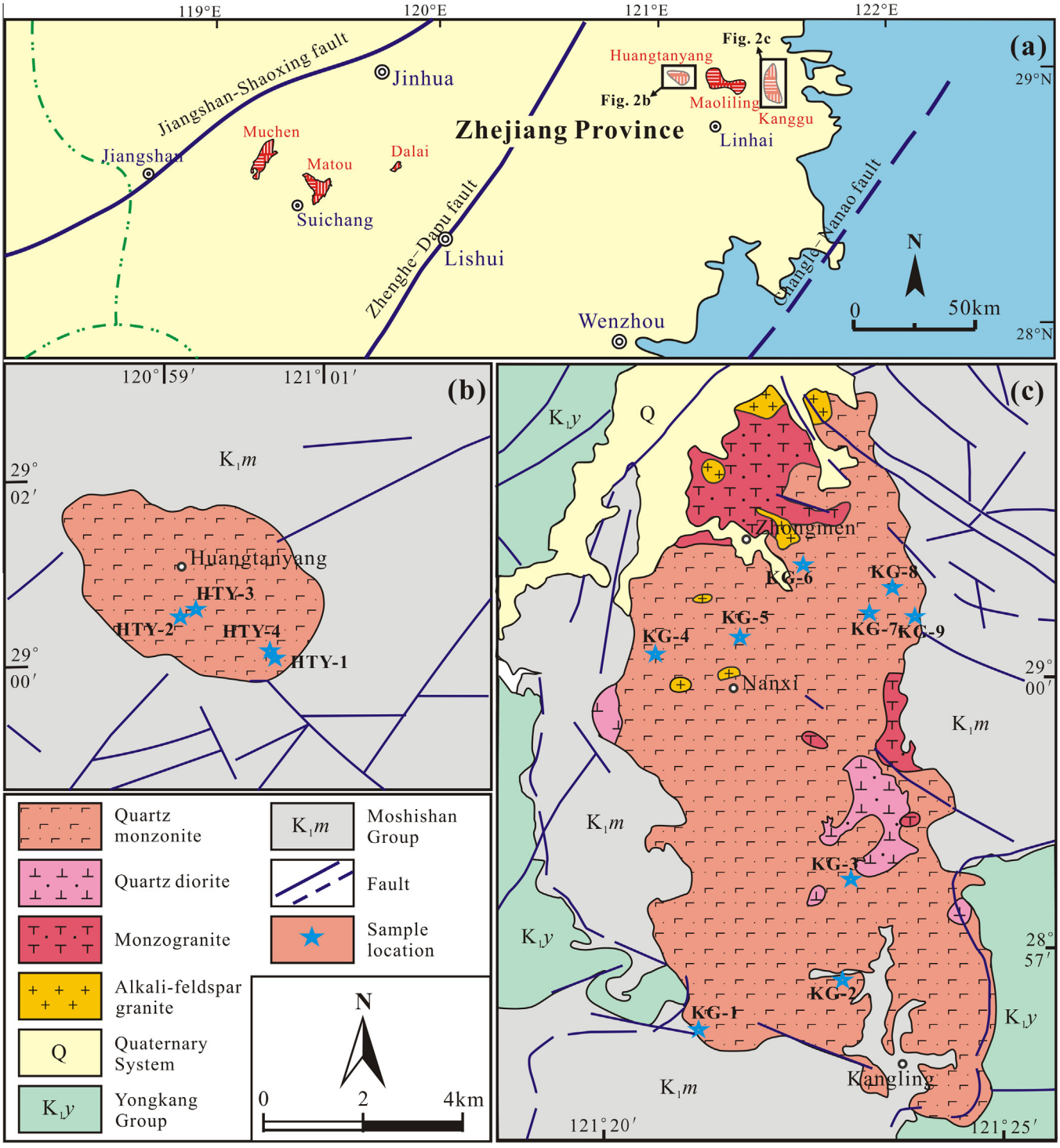

Fig. 2. Simplified geological map of the Huangtanyang and the Kanggu plutons (modified after the Geological Maps of Sanmen Sheet 1:50,000, Linhai sheet 1:200,000 and Xianju sheet 1:200,000).

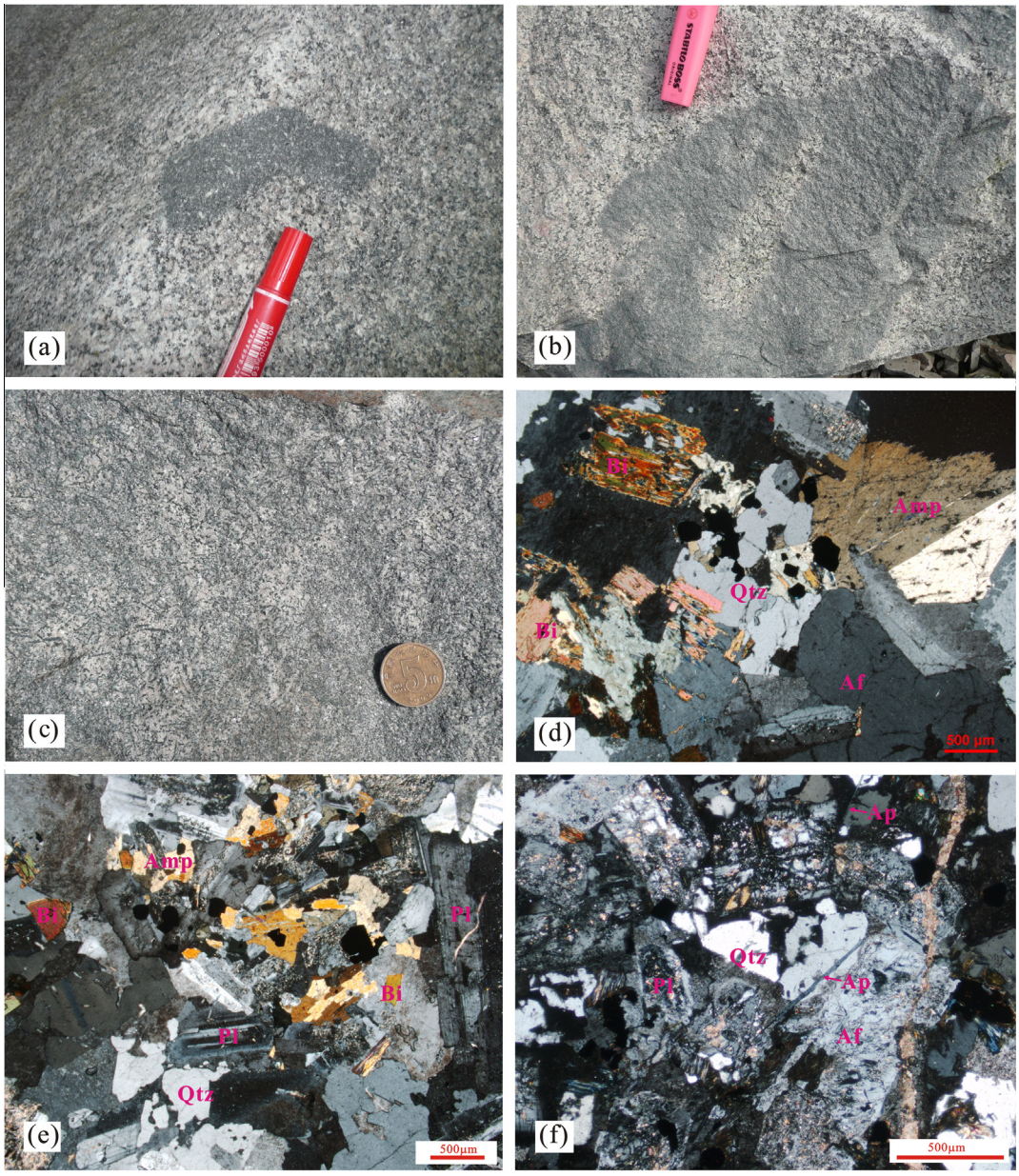

Fig. 3. (a) Macroscopic images of MME with an irregular shape in the Huangtanyang pluton; (b) macroscopic images of host–enclave relationships in the Kanggu pluton; (c) mafic minerals with elongate to acicular forms from the MME in the Kanggu pluton; (d) thin section photograph of representative quartz monzonite from the Huangtanyang pluton; (e) thin section photograph of representative quartz monzonite from the Kanggu pluton; (f) thin section photograph of representative mafic enclave from the Kanggu pluton. All the thin section photographs were taken using a Nikon microscope under cross-polarised light (Qtz = quartz, Af = alkali-feldspar, Pl = plagioclase, Amp = amphibole, Bi = biotite).

monzonites are medium- to fine-grained and consist of plagioclase (40–45%), alkali feldspar (20–23%), quartz (18–20%), hornblende (8–9%), biotite (6–8%) and minor pyroxene, with accessories of zircon, apatite, titanite and magnetite (Fig. 3a). Plagioclase occurs as euhedral to subhedral crystals with compositions ranging from andesine to oligoclase. Amphibole crystals are subhedral to euhedral and show characteristic green[1] to brown pleochroism. Biotite varies in form from anhedral grains to subhedral blade-shaped crystals.

The Kanggu pluton is also within the eastern Cathaysia Block, and occurs from the Zhongmen region of Sanmen County to the Kanggu region of Linhai County, Zhejiang Province. This pluton is exposed as a spindle-shaped body with a total outcrop area of 73 km^2, and intruded the Moshishan Group and Cretaceous volcanic or hypabyssal intrusive rocks of the Yongkang Group (Fig. 2c). Rocks of Kanggu pluton are mainly quartz monzonite and minor quartz diorite and monzogranite. The quartz monzonites are volumetrically the most important part of the pluton and contain abundant MMEs. The quartz monzonites are medium- to fine-grained, and consist of plagioclase (35–50%), alkali feldspar (25–38%), quartz (15–18%), pyroxene (1–3%), hornblende (2–3%), and biotite (1–2%), with minor accessory minerals such as zircon, apatite, titanite, and magnetite (Fig. 3b and c).

Mafic microgranular enclaves (MMEs) are abundant and randomly distributed in both plutons, ranging in shape from spheroidal to irregular and in size from a few centimetres up to several decimeters (Fig. 3a and b). All enclaves are notably

[1] For interpretation of colour in Fig. 3, the reader is referred to the web version of this article.

fine-grained and dark-coloured relative to the host rocks (Fig. 3a and b). The contacts between enclaves and host rocks are mainly rounded and irregular or diffuse, with no evidence of deformation (Fig. 3a and b). Some mafic enclaves with gulfs and embayments present at their margins are observed (Fig. 3b). It is notable that enclaves partially enclose feldspar xenocrysts of the host rocks (Fig. 3a), and MMEs with cores intruded by granitoid magma are common (Fig. 3b). Mafic minerals in the MMEs from the Kanggu pluton occasionally show elongate to acicular forms (Fig. 3c).

Compared with the host monzonite, MMEs generally contain the same mineral assemblage but with higher contents of ferromagnesian minerals and plagioclase, and lower contents of quartz and K-feldspar. The MMEs are mainly monzodioritic in composition and composed of plagioclase (55–60%), alkali feldspar (15%±), quartz (5%±), hornblende (10%±), and biotite (6%), with accessory minerals of zircon, apatite, titanite, and magnetite (Fig. 3f). Textures vary from equigranular to fine-grained and porphyritic. Plagioclase crystals occur as elongate laths both in phenocrysts and in the groundmass, and the phenocrysts show complex oscillatory zoning with repeated resorption surfaces (Fig. 3f). The core or mantle parts from plagioclase crystals are mainly of labradorites and minor andesines, however, the resorption surfaces are mainly of alkali feldspar and oligoclase. K-feldspar and minor quartz occur as anhedral crystals, interstitial to other minerals. Amphiboles are present as subhedral to euhedral phenocrysts and invariably show greenish-brown to reddish-brown pleochroism. Biotite occurs mainly as anhedral to subhedral blade-shaped crystals. Apatites are common accessory mineral in the MMEs, displays euhedral acicular habits with crystals elongated along the "c" crystallographic axis (Fig. 3f), and are indicative of rapid cooling and crystallisation (e.g., Sparks and Marshall, 1986; Vernon et al., 1988).

3. Analytical methods

Fresh samples were prepared in three groups: thin sections for petrography; 200 mesh powder crushed by an agate mill for major, trace element, and Sr–Nd isotope analyses; 40–60 mesh crushings for selecting zircon grains to use for U–Pb dating and Hf analyses.

3.1. Zircon U–Pb dating and Hf isotopes

Zircons from five samples were separated by conventional techniques, including crushing, sieving, and magnetic and heavy liquid separation methods. Single zircon crystals from each sample were handpicked under a binocular microscope on the basis of size, clarity, colour, and morphology. The handpicked crystals were mounted in epoxy resin and polished to expose crystal centres. Prior to analysis, transmitted and reflected light photomicrographs and cathodoluminescence (CL) images were taken to reveal any internal zoning and inheritance. CL images of zircon grains were obtained using a Mono CL3+ detector (manufactured by Gatan, USA) attached an electron microscope (Quanta 400 FEG) at the State Key Laboratory of Continental Dynamics at Northwest University, Xi'an, in order to identify zircon internal textures and select target spots for U–Pb dating and Hf analyses. The operating conditions were 10.0 kV accelerating voltage and 20 nA primary beam current.

Zircon U–Pb isotopic analyses were conducted by laser ablation-inductively coupled plasma-mass spectrometry (LA-ICP-MS) at the State Key Laboratory for Mineral Deposits Research, Nanjing University, China, using an Agilent 7500s ICP-MS coupled to a New Wave Research 213 nm laser ablation system. The laser system delivers a beam of 213 nm ultraviolet light from a frequency-quintupled Nd:YAG laser. The ablated material was transported in a helium carrier gas through PVC tubing (inner diameter = 3 mm) and combined with argon in a 30 cm^3 mixing chamber prior to entering the ICP-MS. Analyses were carried out with a laser beam diameter of 25 μm and repetition rate of 5 Hz. Data acquisition for each analysis took 100 s (40 s on background, 60 s on signal). The raw count rates for ^{206}Pb, ^{207}Pb, ^{208}Pb, ^{232}Th, and ^{238}U were collected for age determination. A homogeneous standard zircon (GEMOC GJ-1; $^{207}Pb/^{206}Pb$ age of 608.5 ± 1.5 Ma; Jackson et al., 2004) was used to correct for the mass discrimination of the mass spectrometer and any elemental fractionation. A near-concordant standard zircon (Mud Tank; intercept age 732 ± 5 Ma; Black and Gulson, 1978) was used as the internal standard to assess the reproducibility and instrument stability. Detailed analytical procedures are similar to those described by Jackson et al. (2004). The raw ICP-MS U–Pb isotopic data were exported in ASCII format and processed using the GLITTER 4.4 software (van Achterbergh et al., 2001). Common Pb corrections were performed using the method described by Andersen (2002). Mean age calculations and plotting of concordia diagrams were performed using Isoplot (version 2.49) (Ludwig, 2001). The concentrations of U and Th in each analysis were derived by comparison of the background-corrected count rates with the mean count rates on the GJ-1 standard, which has well-defined concentrations of these two elements.

In situ zircon Hf isotopic analyses were conducted on the same spots where U–Pb age determinations were made. Hf isotopic compositions were determined with a Thermo Scientific Neptune Plus MC-ICP-MS coupled to a New Wave UP193 solid-state laser ablation system at the State Key Laboratory for Mineral Deposits Research, Nanjing University. Zircons were ablated with a beam diameter of 35 μm, an 8 Hz laser repetition rate, and with an energy of 12.0–13.6 J/cm^2. During Hf isotopic analyses, two reference standards were also analysed: 91,500 zircon ($^{176}Hf/^{177}Hf$ = 0.282290 ± 0.000012, n = 21, 2σ); Mud Tank zircon ($^{176}Hf/^{177}Hf$ = 0.282501 ± 0.000005, n = 37, 2σ). Their $^{176}Hf/^{177}Hf$ ratios agree with the recommended values within 2σ error (Griffin et al., 2007).

3.2. Bulk-rock major and trace element, and Sr–Nd isotope analyses

Whole rock major and trace elements, and Sr–Nd isotopic compositions were determined at the State Key Laboratory for Mineral Deposits Research, Nanjing University. For major element analyses, mixtures of whole rock powders (0.5 g) and $Li_2B_4O_7$ + $LiBO_2$ + LiBr (11 g) were made into glass discs and were analysed using a Thermo Scientific ARL 9900 X-ray fluorescence (XRF). The analytical precision is estimated to be better than 10% for all major elements, with the majority better than 1%. For trace element analyses, about 50 mg of powders were dissolved in high-pressure Teflon bombs using a HF + HNO_3 mixture. Rh was used as an internal standard to monitor signal drift during counting. Trace element concentrations were determined using a Finnigan Element II ICP-MS. The precision of ICP-MS analyses is better than 10% for all trace elements, with the majority better than 5%. Detailed analytical procedures for the trace element analyses are described by Gao et al. (2003).

Sr isotopic compositions were measured using a Finnigan Triton TI thermal ionisation mass spectrometer (TIMS) following the methods of Pu et al. (2004, 2005), whereas Nd isotopic compositions were measured using a Thermo Scientific Neptune Plus MC-ICP-MS. For whole-rock Sr–Nd isotope analyses, ca. 50 mg of powder was dissolved in the same way as for trace element analyses. Rb–Sr and Sm–Nd has been separated by adopting resin of AG50W×8 and different eluent reagents. Firstly, REEs are separated from Rb–Sr by using normal method of cation-exchange chromatography with eluent of HCl. Then Rb and Sr are separated and purified by using a mixed eluent of pyridinium

and DCTA complex. Sm and Nd are separated and purified by using HIBA as an eluent through a very small volume of cation-exchange resin (0.6 mL). $^{87}Sr/^{86}Sr$ and $^{143}Nd/^{144}Nd$ ratios are reported as measured, after normalisation to $^{86}Sr/^{88}Sr = 0.1194$ and $^{146}Nd/^{144}Nd = 0.7219$, respectively, to correct for instrumental fractionation. During the period of this study, measurements of the Japan JNdi-1 Nd standard gave $^{143}Nd/^{144}Nd = 0.512096 \pm 0.000008$ ($n = 18$; 2σ) and for the NIST SRM 987 Sr standard gave $^{87}Sr/^{86}Sr = 0.710248 \pm 0.000004$ (2σ).

4. Results

4.1. Zircon U–Pb geochronology

Five samples (HTY-2, KG-3h, KG-3g, KG-5 and KG-3e) from the Huangtanyang and Kanggu plutons are selected for LA-ICP-MS zircon U–Pb dating. CL images of representative zircon grains are shown in Fig. 4. The results of LA-ICP-MS U–Pb isotopic analyses are given in Appendix 1 and are presented graphically in Figs. 5 and 6. Because of counting statistics, $^{207}Pb/^{206}Pb$ isotopic ages are more precise for older (>1.0 Ga) zircons, while $^{206}Pb/^{238}U$ ages are more precise for younger zircons (Compston et al., 1992; Griffin et al., 2004). Therefore, we use the $^{206}Pb/^{238}U$ ages for the younger zircons from Appendix 1 in the following discussion.

4.1.1. Huangtanyang quartz monzonites

Zircon crystals from the Huangtanyang quartz monzonites (HTY-2) are commonly transparent, colourless to pale yellow, euhedral to subhedral prismatic, and 80–300 μm in length with length/width ratios of 1:1 to 4:1. All grains exhibit regular magmatic oscillatory zoning with no inherited cores in CL images (Fig. 4a), and have high Th/U ratios (Th/U = 1.37–2.12; Appendix 1), implying a magmatic origin (Hoskin and Schaltegger, 2003; Wu and Zheng, 2004). Twenty-four analyses from HTY-2 form a concordant group with a weighted mean $^{206}Pb/^{238}U$ ages of 108.4 ± 1.5 Ma (MSWD = 1.9; 2σ) (Fig. 5), which is regarded as the emplacement age of Huangtanyang quartz monzonites.

4.1.2. Kanggu quartz monzonites

Zircons grains from the Kanggu quartz monzonites (KG-3h, KG-3g and KG-5) are colourless to pale brown, transparent, euhedral prismatic to elongated prismatic, with lengths of 80–350 μm and length/width ratios of 1:1 to 4:1. All zircon grains show typical magmatic oscillatory zoning or occasional typical absorption zoning in CL images (Fig. 4b), and have high Th/U ratios (Th/U = 0.95–3.16; Appendix 1). Twenty-five analyses from KG-3h are all concordant or near-concordant, yielding a weighted mean $^{206}Pb/^{238}U$ ages of 109.0 ± 1.4 Ma (MSWD = 1.4; 2σ) (Fig. 6a). Twenty-four analyses from KG-3 g give consistent results, with a weighted mean $^{206}Pb/^{238}U$ ages of 108.9 ± 1.0 Ma (MSWD = 1.06; 2σ) (Fig. 6b). Twenty-one concordant analyses from KG-5 yield weighted mean $^{206}Pb/^{238}U$ ages of 104.6 ± 0.9 Ma (MSWD = 0.88; 2σ) (Fig. 6c). Thus, the emplacement age of the Kanggu quartz monzonites is suggested to be 105–109 Ma.

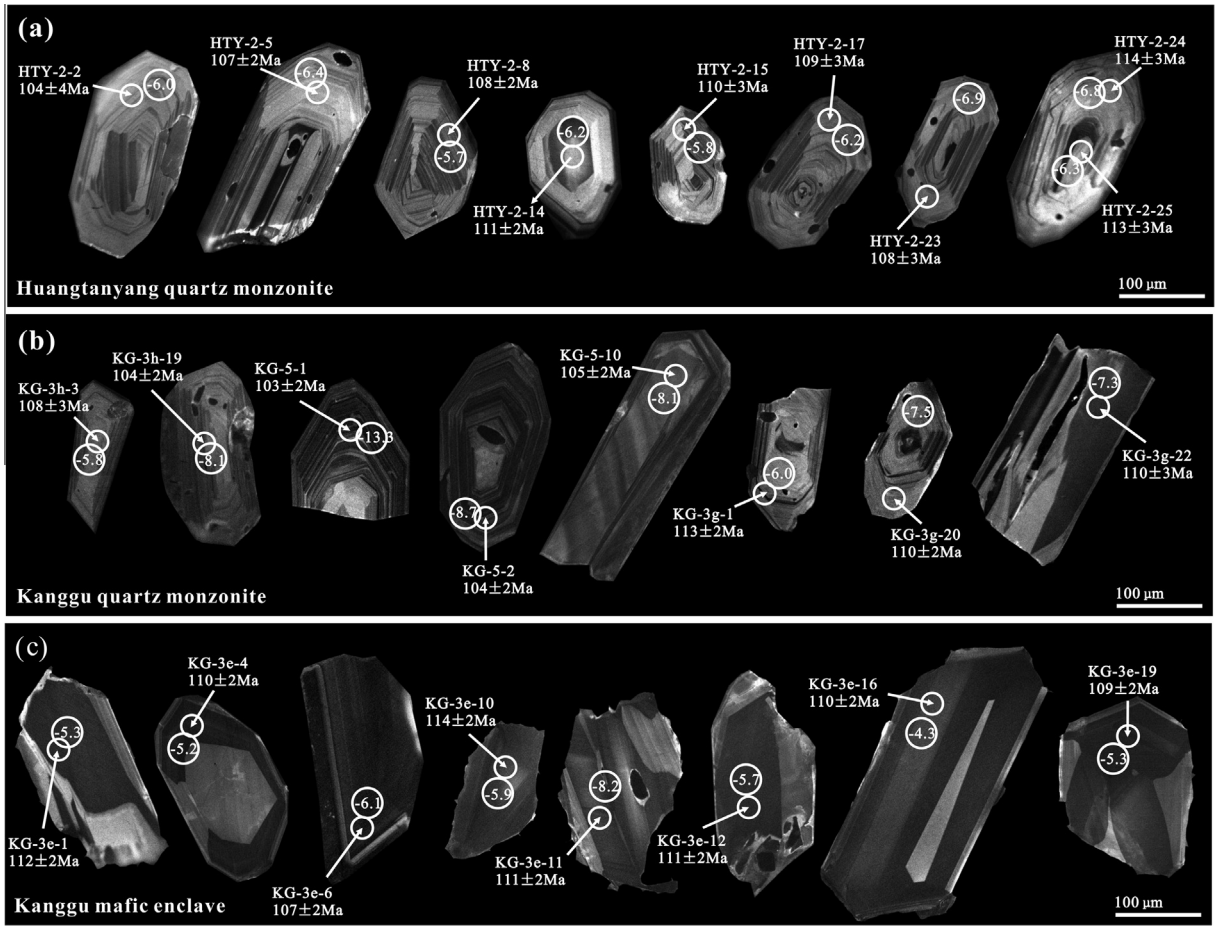

Fig. 4. Representative cathodoluminescence (CL) images of selected zircons from Huangtanyang and Kanggu plutons. The morphology of zircon grains, $^{206}Pb/^{238}U$ ages, and $\varepsilon_{Hf}(t)$ values are shown. Small circles indicate the U–Pb dating positions, and large circles indicate the sites for Hf isotope analysis, with circle diameters showing the approximate laser spot sizes.

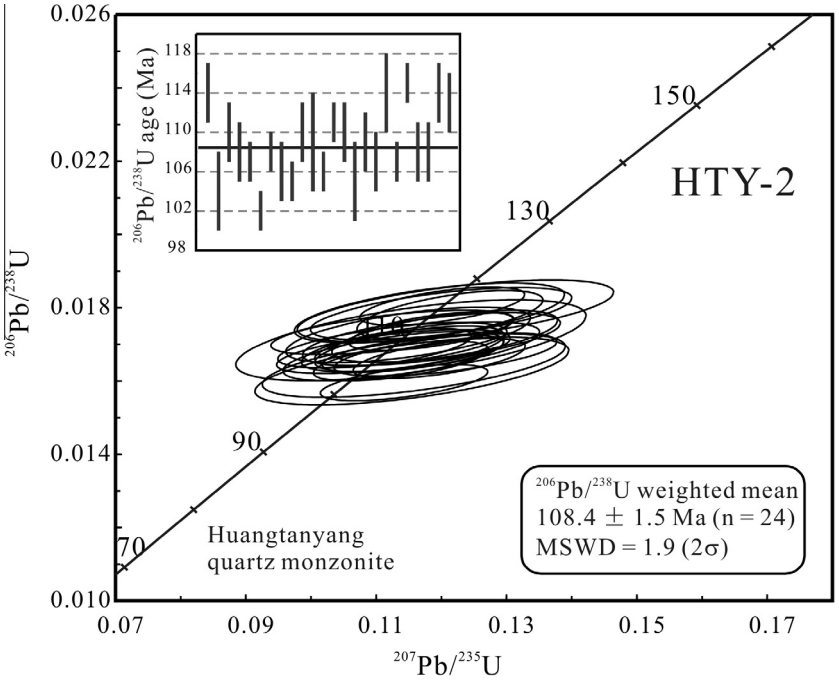

Fig. 5. Zircon U–Pb concordia diagrams for quartz monzonites from the Huangtanyang pluton.

4.1.3. MME within the Kanggu pluton

Zircon grains from mafic microgranular enclave (KG-3e) are colourless and transparent, euhedral to subhedral, stubby to prismatic, 100–400 μm in length with length/width ratios of 1:1 to 2.5:1. All zircon grains generally show typical absorption zoning and occasional weak magmatic oscillatory zoning in CL images (Fig. 4c), and have higher Th/U ratios (Th/U = 2.72–5.00; Appendix 1) than those of host rocks. Twenty analyses from KG-3e all plot on the concordia curve and yield a weighted mean $^{206}Pb/^{238}U$ ages of 109.9 ± 1.1 Ma (MSWD = 1.3; 2σ) (Fig. 6d), which is interpreted as the crystallisation age of MMEs. The results agree with sample from host rocks (KG-3h), which indicate that the enclave-forming magmas are coeval with their host monzonitic magmas.

4.2. Major and trace element geochemistry

The whole-rock major and trace element compositions of representative samples from the Huangtanyang and Kanggu plutons are given in Tables 1 and 2. All the monzonites from Huangtanyang and Kanggu plutons have an intermediate-acidic signature (SiO_2 = 61.35–66.22 wt.%) and moderately to relatively high alkali contents ($K_2O + Na_2O$ = 7.34–8.22 wt.%), which fall in the quartz monzonite or monzonite fields and subalkaline series on a total alkalis vs. silica (TAS) diagram (Fig. 7a). Data for most samples plot in the alkali-calcic fields on a ($K_2O + Na_2O$–CaO) *vs.* SiO_2 diagram (Fig. 7b). All the monzonites from Huangtanyang and Kanggu plutons are enriched in K_2O with K_2O/Na_2O ratios of 0.66–1.04, and fall within the high-K calc-alkaline series on a SiO_2–K_2O diagram (Fig. 7c). These monzonites have relatively low concentrations of CaO (2.66–4.06 wt.%), TiO_2 (0.53–0.79 wt.%), and P_2O_5 (0.20–0.30 wt.%), and have much lower FeO^T/MgO ratios (2.17–2.78) than A-type granites (mean FeO^T/MgO = 13.4; Whalen et al., 1987). They possess relatively low A/CNK values of 0.89–0.96 (Table 1; Fig. 7d), and display metaluminous characteristics. Chondrite-normalised rare earth element (REE) patterns of these monzonites show relative enrichment of light REEs, and relatively low in heavy REE concentrations, with variable high $(La/Yb)_N$ ratios (6.39–29.59) and slightly negative or no Eu anomalies (δEu = 0.78–1.02) (Fig. 8a). In primitive mantle-normalised multi-element plots (Fig. 8b), all the monzonites have negative anomalies of Nb, Ta, P and Ti, and pronounced positive anomalies of Ba, Th, U, Pb, Zr and Hf. In addition, they show similar trace element characteristics to the Cretaceous basaltic rocks in the coastal region of Cathaysia Block (100–77 Ma), but have relatively enrichment of light REEs such as La and Ce (Fig. 8).

In contrast, MME from Kanggu pluton is intermediate in composition with SiO_2 contents of 58.51 wt.%, and plots in the monzonite field (Fig. 7a). It has similar K_2O contents and K_2O/Na_2O ratios (K_2O/Na_2O = 0.79) to the host rocks, but show higher $Fe_2O_3^T$ (6.06 wt.%), MgO (2.29 wt.%), and P_2O_5 (0.48 wt.%). Chondrite-normalised REE patterns for the MME is marked by enrichment in the LREEs and weakly negative Eu anomalies (δEu = 0.92) (Fig. 8a). Notably, the MME displays similar high total REE concentrations (∑REE = 262.4 ppm) and sub-parallel REE patterns to its host rocks. In primitive mantle-normalised multi-element plots (Fig. 8b), the sample from MME shows enrichments in Rb, Th, U, K, and light REEs, and depletions in Nb, Ta, and Ti, which are similar to those of the host rocks. However, the MME does not exhibit pronounced negative Sr and P anomalies.

4.3. Sr–Nd isotopic compositions

Whole-rock Sr–Nd isotopic compositions of representative samples from the Huangtanyang and Kanggu plutons are given in Table 3 and Fig. 9. Initial $^{87}Sr/^{86}Sr$ ratios (I_{Sr}) and $\varepsilon_{Nd}(t)$ values were calculated using their zircon U–Pb ages obtained in this study. The Huangtanyang and Kanggu quartz monzonites have uniform initial I_{Sr} values (0.7084–0.7090) and $\varepsilon_{Nd}(t)$ values (−7.50 to −6.84). In addition, MME from Kanggu pluton has similar Sr and Nd isotopic compositions to its host tocks, with I_{Sr} values of 0.7089 and $\varepsilon_{Nd}(t)$ values of −7.16. All of the rocks have relatively young two-stage Nd model ages (T_{DM2}; 1.47–1.53 Ga). It is notable that the Sr–Nd isotopic compositions of the Huangtanyang and Kanggu plutons

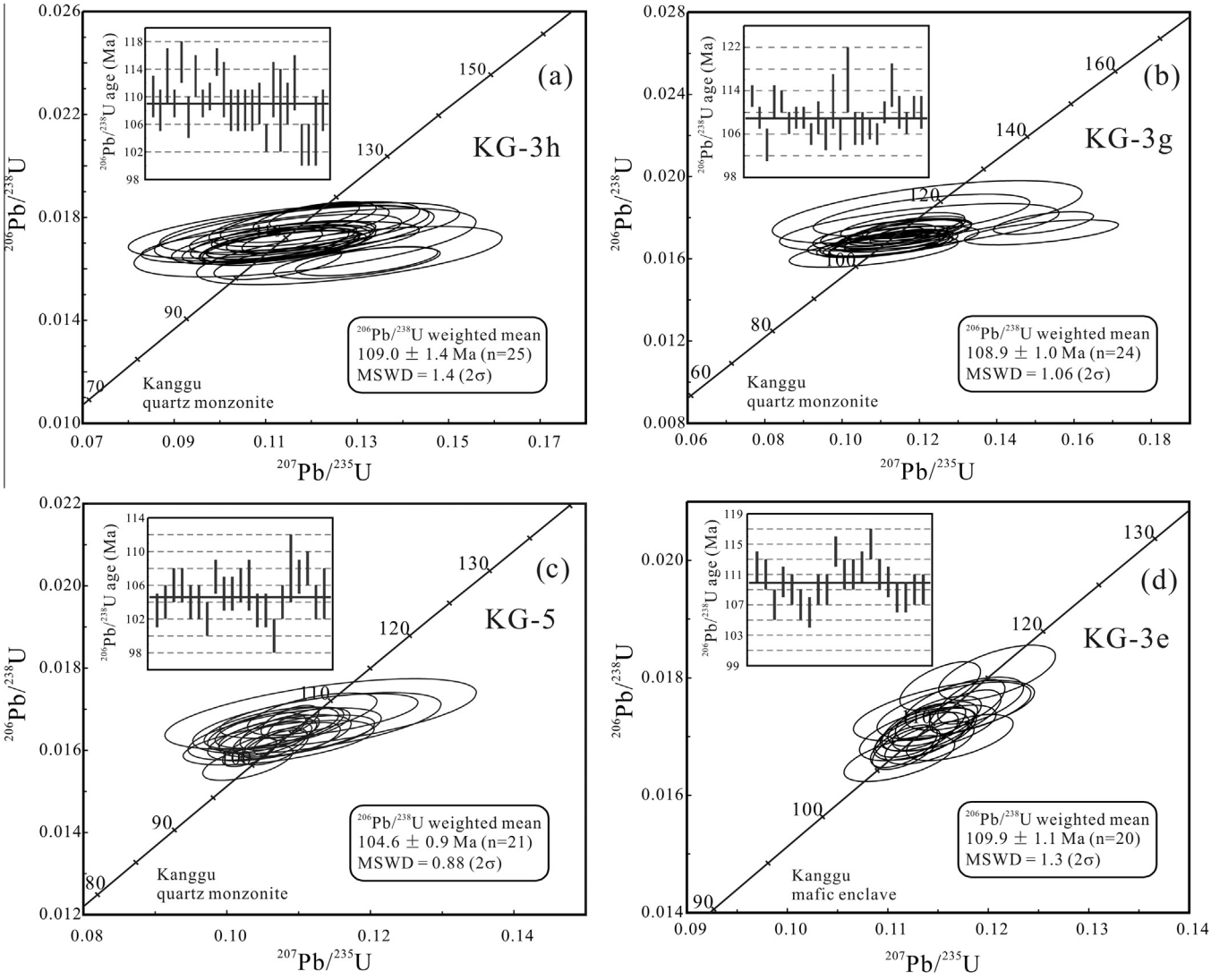

Fig. 6. Zircon U–Pb concordia diagrams for quartz monzonite (a–c) and MMEs (d) from the Kanggu pluton.

Table 1
Major element contents (wt.%) of representative samples from the Huangtanyang and the Kanggu plutons.

Rock type	Huangtanyang quartz monzonites				Kanggu quartz monzonites								Kanggu enclaves
Sample	HTY-1	HTY-2	HTY-3	HTY-4	KG-1	KG-2	KG-3h	KG-3g	KG-4	KG-5	KG-7	KG-8	KG-3e
SiO_2	63.77	64.73	66.22	63.30	64.33	63.48	61.35	64.71	62.33	64.15	64.94	65.32	58.51
TiO_2	0.69	0.64	0.53	0.71	0.64	0.71	0.79	0.60	0.74	0.65	0.64	0.63	0.83
Al_2O_3	15.37	15.20	15.04	15.91	15.95	15.84	16.48	15.39	15.77	15.70	15.49	15.62	16.15
$Fe_2O_3^T$	4.74	4.45	3.67	4.83	4.08	4.59	5.22	3.80	5.19	4.38	4.18	4.13	6.06
MnO	0.10	0.11	0.08	0.10	0.07	0.10	0.11	0.08	0.10	0.08	0.11	0.17	0.12
MgO	1.82	1.64	1.36	2.00	1.45	1.70	1.79	1.31	2.02	1.60	1.45	1.34	2.29
CaO	3.82	3.47	3.26	4.06	2.90	3.70	3.99	2.66	3.99	3.79	3.26	3.20	4.84
Na_2O	3.83	3.87	3.70	3.95	4.43	3.95	4.63	4.50	3.90	4.18	4.17	3.89	4.08
K_2O	3.52	4.01	3.79	3.39	3.78	3.63	3.04	3.72	3.60	3.39	3.82	3.89	3.21
P_2O_5	0.25	0.22	0.20	0.26	0.23	0.26	0.30	0.22	0.25	0.23	0.22	0.21	0.48
LOI	0.90	0.49	0.84	0.61	1.16	0.98	1.52	2.16	0.96	0.70	0.78	1.08	2.31
Total	98.81	98.83	98.68	99.14	99.02	98.94	99.22	99.15	98.84	98.85	99.06	99.48	98.90
FeO^T/MgO	2.35	2.45	2.43	2.17	2.53	2.43	2.62	2.60	2.31	2.47	2.60	2.78	2.38
Mg#	43.2	42.1	42.3	45.1	41.3	42.3	40.4	40.7	43.5	41.9	40.7	39.1	42.8
K_2O/Na_2O	0.92	1.04	1.02	0.86	0.85	0.92	0.66	0.83	0.92	0.81	0.92	1.00	0.79
ALK	7.35	7.89	7.49	7.34	8.21	7.58	7.67	8.22	7.50	7.57	7.99	7.78	7.30
A/CNK	0.90	0.89	0.93	0.91	0.96	0.92	0.91	0.94	0.90	0.90	0.91	0.95	0.85
AKI	0.66	0.71	0.68	0.64	0.71	0.66	0.66	0.74	0.65	0.67	0.71	0.68	0.63
A/NK	1.52	1.42	1.47	1.56	1.40	1.52	1.51	1.34	1.53	1.49	1.41	1.47	1.58
A.R	2.24	2.42	2.36	2.16	2.54	2.27	2.20	2.67	2.22	2.27	2.49	2.41	2.07
D.I.	73.23	76.12	77.45	71.53	77.96	73.65	71.77	79.92	71.48	74.49	77.32	76.88	66.88

$Fe_2O_3^T$, total Fe; LOI, loss on ignition; Mg# = 100 * mol MgO/(mol MgO + FeO); A/CNK = mol Al_2O_3/(mol Na_2O + K_2O + CaO); AKI = (mol Na_2O + K_2O)/mol Al_2O_3.

Table 2
Trace and rare earth element (ppm) analyses of representative samples from Huangtanyang and Kanggu plutons.

Rock type	Huangtanyang quartz monzonites				Kanggu quartz monzonites								Kanggu enclaves
Sample	HTY-1	HTY-2	HTY-3	HTY-4	KG-1	KG-2	KG-3h	KG-3g	KG-4	KG-5	KG-7	KG-8	KG-3e
Sc	10.15	9.69	8.49	11.27	7.74	9.41	10.61	7.20	11.84	9.29	9.00	8.43	10.57
V	116	104	89	125	100	115	125	86	145	112	99	94	141
Cr	12.89	12.10	14.80	13.83	2.91	3.98	3.27	5.02	9.16	5.32	3.12	3.58	5.04
Co	10.45	10.48	8.22	10.40	8.67	11.37	11.86	7.37	12.17	9.31	8.63	8.36	14.58
Ni	7.26	7.47	8.78	7.61	2.71	4.50	2.93	3.49	6.89	4.74	2.77	3.22	4.38
Ga	22.23	21.12	20.32	22.92	22.07	22.03	24.35	22.17	23.24	22.73	22.57	23.05	24.42
Rb	165	188	190	164	163	137	119	164	178	148	185	191	132
Sr	498	473	442	568	618	640	735	542	593	558	526	540	790
Y	19.75	17.11	17.61	19.76	17.68	18.76	19.07	18.09	18.75	19.69	18.72	19.78	22.21
Zr	261	277	222	284	317	340	366	336	277	285	315	335	256
Nb	14.26	12.25	12.67	12.80	12.64	12.51	12.37	12.89	11.89	12.64	13.11	14.03	11.20
Ba	1096	1105	1021	1204	1343	1302	1212	1197	1114	1036	1199	1207	1181
Hf	6.77	6.61	5.71	6.88	8.02	8.44	9.55	8.71	7.90	7.81	8.43	8.72	6.55
Ta	1.06	0.91	0.98	0.89	0.88	0.86	0.79	0.90	0.84	0.93	0.90	0.99	0.68
Pb	22.03	32.75	14.72	23.62	15.19	15.38	21.07	17.64	15.74	16.90	33.28	63.07	19.73
Th	20.22	20.22	20.73	16.81	19.51	20.30	15.92	21.98	21.23	20.68	21.48	24.06	16.95
U	4.65	3.27	5.78	3.91	3.93	3.10	2.99	4.41	4.11	4.83	4.91	3.76	3.91
La	45.74	21.66	20.65	108.67	52.88	54.19	52.07	51.90	41.38	42.96	57.51	57.15	60.23
Ce	80.06	44.85	43.98	183.48	95.47	103.95	97.46	97.80	83.39	83.29	109.58	107.80	113.69
Pr	9.37	5.11	5.05	18.63	10.45	10.86	10.63	10.39	9.01	9.71	11.46	11.40	12.92
Nd	34.61	21.40	20.76	61.23	37.03	37.21	40.65	37.11	34.80	36.01	40.89	40.88	47.45
Sm	5.67	4.20	4.21	7.59	5.46	5.88	6.41	5.78	5.83	6.09	6.33	6.22	7.55
Eu	1.48	1.31	1.28	1.64	1.50	1.59	1.80	1.41	1.55	1.53	1.55	1.57	1.95
Gd	4.48	3.69	3.56	5.41	4.23	4.60	4.93	4.26	4.61	4.68	4.77	4.73	5.59
Tb	0.59	0.50	0.49	0.65	0.58	0.61	0.63	0.57	0.62	0.63	0.65	0.62	0.70
Dy	3.83	3.27	3.32	4.12	3.69	3.83	4.10	3.73	4.09	4.04	3.95	3.98	4.64
Ho	0.84	0.72	0.75	0.86	0.78	0.85	0.87	0.81	0.90	0.89	0.91	0.87	1.02
Er	2.56	2.20	2.29	2.60	2.34	2.54	2.68	2.44	2.69	2.74	2.55	2.63	2.97
Tm	0.36	0.31	0.33	0.37	0.35	0.35	0.36	0.36	0.38	0.39	0.38	0.38	0.43
Yb	2.61	2.06	2.18	2.48	2.30	2.55	2.37	2.43	2.61	2.67	2.63	2.63	2.87
Lu	0.38	0.31	0.34	0.37	0.33	0.38	0.36	0.37	0.38	0.40	0.39	0.40	0.43
∑REE	192.6	111.6	109.2	398.1	217.4	229.4	225.3	219.4	192.2	196.0	243.5	241.2	262.4
δEu	0.90	1.02	1.01	0.78	0.96	0.93	0.98	0.87	0.91	0.88	0.86	0.88	0.92
$(La/Yb)_N$	11.83	7.08	6.39	29.59	15.50	14.35	14.83	14.37	10.68	10.85	14.76	14.68	14.13
$(La/Sm)_N$	5.08	3.25	3.08	9.01	6.09	5.79	5.11	5.64	4.46	4.44	5.72	5.78	5.02
$(Gd/Yb)_N$	1.39	1.44	1.32	1.77	1.48	1.46	1.68	1.41	1.42	1.41	1.47	1.45	1.57
Nb/U	3.07	3.75	2.19	3.27	3.22	4.03	4.13	2.92	2.89	2.62	2.67	3.73	2.86
Ce/Pb	3.63	1.37	2.99	7.77	6.29	6.76	4.63	5.54	5.30	4.93	3.29	1.71	5.76
Ta/U	0.23	0.28	0.17	0.23	0.22	0.28	0.26	0.20	0.20	0.19	0.18	0.26	0.17
t_{Zr} (°C)	798	803	793	804	824	824	824	830	799	806	819	831	/

t_{Zr} (°C), zircon saturation temperature.

are all similar to those of Cretaceous rhyolites or basalts in Zhejiang Province (Fig. 9).

4.4. Zircon Hf isotopic compositions

In situ Hf isotopic compositions of zircons from the Huangtanyang and Kanggu plutons are listed in Appendix 2 and graphically presented in Figs. 10 and 11. For the calculation of $\varepsilon_{Hf}(t)$ and T_{DM2} values, *in situ* zircon U–Pb ages of each zircon were used. It is clear that zircons from the Huangtanyang and Kanggu quartz monzonites have a similar Hf isotopic nature. They are characterised by highly variable zircon Hf isotopic compositions, with $\varepsilon_{Hf}(t)$ values ranging from −8.6 to −5.7 and −13.3 to −5.8 for Huangtanyang and Kanggu quartz monzonites, respectively (Appendix 2). In contrast, the MME samples have relatively depleted zircon Hf isotopic compositions with $\varepsilon_{Hf}(t)$ values varying from −8.4 to −3.8. On a plot of $\varepsilon_{Hf}(t)$ vs. t (Fig. 10), most of samples plot above the fields of the Hf isotope evolutionary area for the crustal basement in the Cathaysia Block. Moreover, most zircons also have younger two-stage Hf model ages (T_{DM2} (Hf); 1.50–1.69 Ga, 1.51–1.97 Ga and 1.38–1.67 Ga for Huangtanyang quartz monzonites, Kanggu quartz monzonites and MMEs, respectively) than those of the basement metamorphic rocks in Cathaysia Block (1.8–2.2 Ga; Chen and Zhou, 1999).

5. Discussion

5.1. Origin of the MMEs

There are three main interpretations regarding the origin of mafic microgranular enclaves (MMEs), including: (1) fragments of recrystallised, refractory metamorphic rocks or melt residues from the granite source (e.g., Chappell et al. 1987; Chen et al., 1989; Chappell and White, 1992; White et al., 1999); (2) cognate fragments of cumulate minerals or early-formed crystals from the host magma (e.g., Noyes et al., 1983; Chappell et al., 1987; Clemens and Wall, 1988; Dahlquist, 2002; Donaire et al., 2005; Ilbeyli and Pearce, 2005; Shellnutt et al., 2010); (3) globules of a more mafic magma that were injected into and mingled with the felsic magma (e.g., Vernon, 1984; Dorais et al., 1990; Blundy and Sparks, 1992; Wiebe et al., 1997; Kadioglu and Gulec, 1999; Perugini et al., 2003; Barbarin, 2005; Kocak, 2006; Hawkesworth and Kemp, 2006; Yang et al., 2006, 2007; Feeley et al., 2008; Chen et al., 2009; Kocak et al., 2011; Cheng et al., 2012; Jiang et al., 2012; Lan et al., 2013; Liu et al., 2013, 2014b; Feng et al., 2014).

The resitite model has long been favoured for the origin of enclaves, which would result in the MMEs having a metamorphic or residual sedimentary fabric (Chappell et al., 1987; White et al., 1999). For the studied enclaves from Huangtanyang and Kanggu plutons, the absence of these fabrics argues against a residual

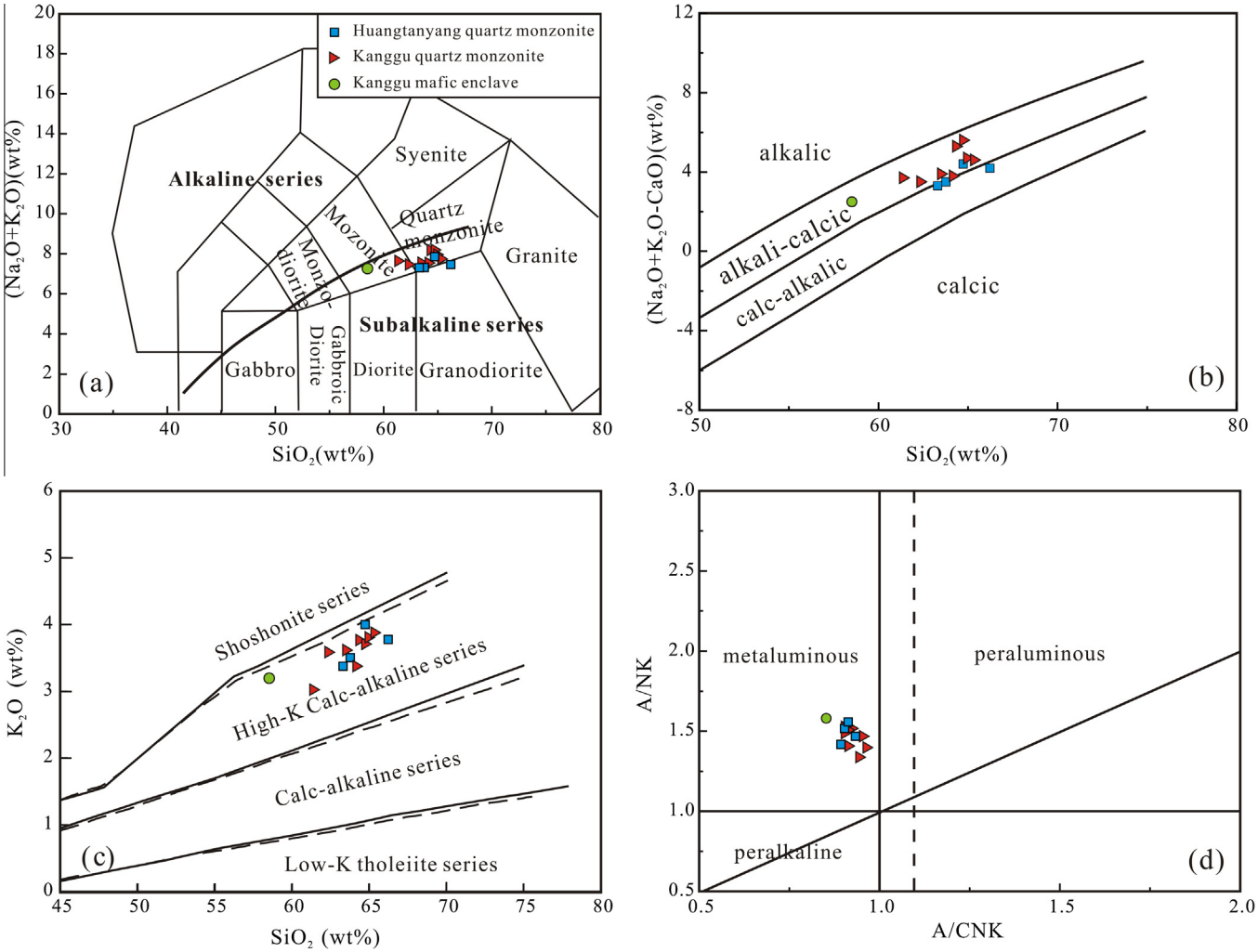

Fig. 7. Chemical classification of rocks from the Huangtanyang and Kanggu plutons. (a) Total alkali *vs.* silica (TAS) diagram (Middlemost, 1994; with the thick solid line from Irvine and Baragar, 1971); (b) ($K_2O + Na_2O–CaO$) *vs.* SiO_2 diagram (Frost et al., 2001); (c) K_2O vs. SiO_2 diagram (solid lines from Peccerillo and Taylor, 1976; dashed lines from Middlemost, 1985); (d) A/NK *vs.* A/CNK diagram (Chappell and White, 1974; Maniar and Piccoli, 1989).

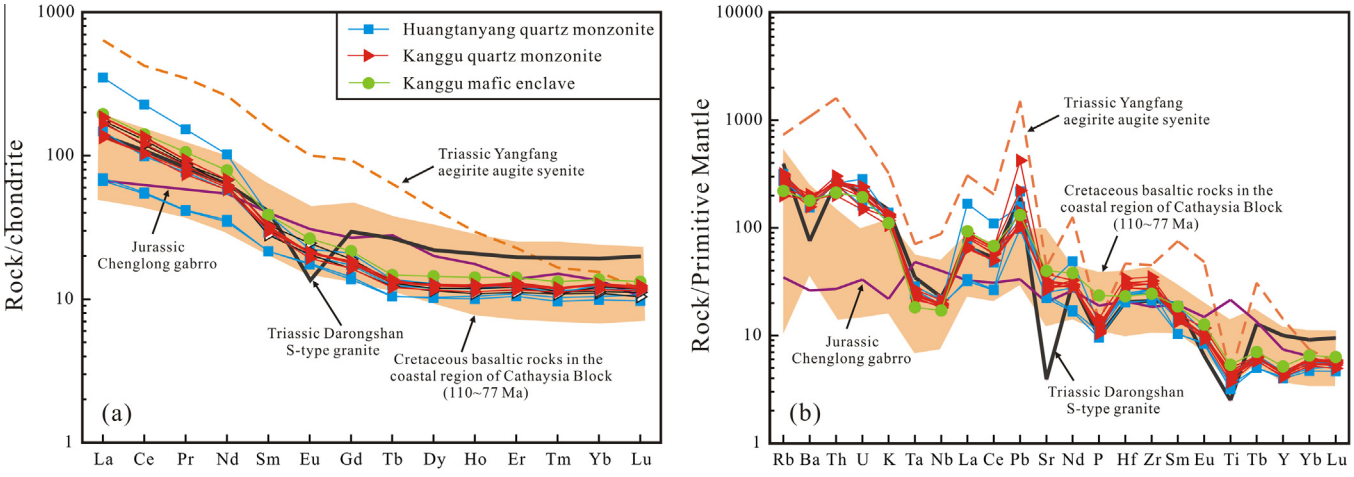

Fig. 8. Chondrite-normalised REE (a; normalisation values from Boynton, 1984) and primitive mantle-normalised multi-element patterns (b; normalisation values from McDonough and Sun, 1995) for rocks from the Huangtanyang and Kanggu plutons. The values for the Cretaceous basaltic rocks in the coastal region of Cathaysia Block are from Chen et al. (2008) and Meng et al. (2012). Comparative data are also shown for the Jurassic Chenglong gabbro (He et al., 2010), Triassic Yangfang aegirite augite syenite (Wang et al., 2005), and Triassic Darongshan S-type granite (Hsieh et al., 2008).

Table 3
Rb–Sr and Sm–Nd isotopic data for Huangtanyang and Kanggu pluton.

Sample no.	t (Ma)	Rb ($\times10^{-6}$)	Sr ($\times10^{-6}$)	$^{87}Rb/^{86}Sr$	$^{87}Sr/^{86}Sr$	I_{Sr}	$^{147}Sm/^{144}Nd$	$^{143}Nd/^{144}Nd$	$\varepsilon_{Nd}(t)$	T_{DM2} (Ga)
Huangtanyang quartz monzonites										
HTY-2	108	187.56	472.55	1.148	0.710120 ± 4	0.708357	0.119	0.512214 ± 5	−7.05	1.49
HTY-4	108	163.60	567.56	0.834	0.709788 ± 6	0.708508	0.075	0.512194 ± 7	−6.84	1.47
Kanggu quartz monzonites										
KG-3h	109	119.26	735.20	0.469	0.709711 ± 4	0.708984	0.095	0.512174 ± 5	−7.50	1.53
KG-3g	109	164.41	542.40	0.877	0.710191 ± 4	0.708832	0.094	0.512184 ± 5	−7.29	1.51
KG-5	105	147.95	557.58	0.768	0.710021 ± 4	0.708875	0.102	0.512188 ± 5	−7.37	1.52
KG-7	109	185.11	525.83	1.019	0.710345 ± 4	0.708767	0.093	0.512178 ± 6	−7.39	1.52
Kanggu enclave										
KG-3e	110	132.13	790.47	0.484	0.709641 ± 5	0.708885	0.096	0.512191 ± 5	−7.16	1.50

$\varepsilon_{Nd}(t)$ values are calculated by granitoid ages and based on ^{147}Sm decay constant of 6.54×10^{-12}, the $^{143}Nd/^{144}Nd$ and $^{147}Sm/^{144}Nd$ ratios of chondrite and depleted mantle at present day are 0.512630 and 0.1960, 0.513151 and 0.2136, respectively (Miller and O'Nions, 1985; Bouvier et al., 2008). T_{DM2} ages are calculated according to the two-stage model as presented by Wu et al. (2003).

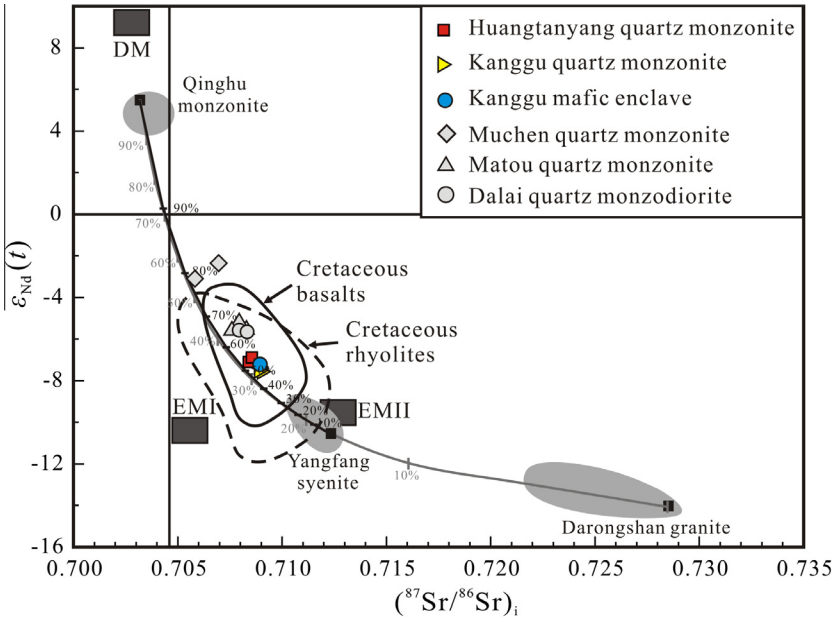

Fig. 9. $\varepsilon_{Nd}(t)$ *vs.* $(^{87}Sr/^{86}Sr)_i$ diagram for the Huangtanyang and Kanggu plutons. Comparative data are shown for the Muchen quartz monzonites (Liu et al., 2013), Matou quartz monzonite and Dalai quartz monzodiorite (Liu et al., 2014b). Also shown are calculated binary mixing curves between possible mafic and felsic magma end-members. Depleted mantle is represented by the Qinghu monzonite in Guangxi Province (Li et al., 2004). Lithospheric mantle is represented by the Yangfang aegirine–augite syenite in western Fujian Province (Wang et al., 2005). The crustal end-member is represented by the Darongshan S-type granite (Hsieh et al., 2008). Tick marks represent 10% mixing increments.

source origin. In addition, no inherited zircon has been found in enclaves of the Kanggu pluton, which is inconsistent with the restite model (Chappell et al., 1987; Chappell et al., 2000; Chen et al., 1989; White et al., 1999). The consistent zircon U–Pb ages between enclaves and host quartz monzonites from the Kanggu plutons as described above also rule out this possibility.

The studied MMEs have similar mineral assemblages and isotopic ages to their host monzonites, therefore could be ascribed to either cognate or hybrid origin. Considering that mineral grains of the studied enclaves are much smaller than those of host monzonites, and no cumulate textures have been observed, we therefore suggest that the MMEs were not generated via cumulate fractional crystallization (Kumar et al., 2004). The similar total REE concentrations and sub-parallel REE patterns between enclaves and their host quartz monzonites from Kanggu pluton are also inconsistent with the autolith model. Furthermore, zircons from the Kanggu enclaves generally have relatively high $\varepsilon_{Hf}(t)$ values on average (mean = −6.1 ± 0.7, n = 20; Appendix 2) than those in host quartz monzonites (−7.8 ± 0.6, n = 70; Appendix 2). Accordingly, we suggest that the studied enclaves cannot be cognate fragments of cumulates or early-formed concretionary bodies from the host magma.

MMEs can also form by a more mafic magmatic component into a cooler felsic magma chamber via a mixing/mingling process. In this model, MMEs represent small batches of mantle-derived mafic melt which once injected into the felsic magma, cool rapidly, partially crystallize and become more viscous to form discrete magma blobs. Integrated field and geochemical characteristics indicate that MMEs from the Huangtanyang and Kanggu plutons were likely generated by this mechanism. Firstly, abundant petrological observations (e.g., the fine-grained textures and irregular chilled margins observed from some large enclaves; enclaves with spheroidal to ellipsoidal–ovoidal shapes and with cores intruded by felsic magma; mafic minerals in the enclaves show elongate to acicular forms; Fig. 3a–c) supports the interpretation that the enclaves represent globules of near-liquidus hot mafic melt that have been injected into and mingled with the host cooler felsic magma (Blundy and Sparks, 1992; Lowell and Young, 1999; Cheng et al., 2012; J.X. Li et al., 2014). Microstructural observations also demonstrate that the MMEs were globules of mafic magma

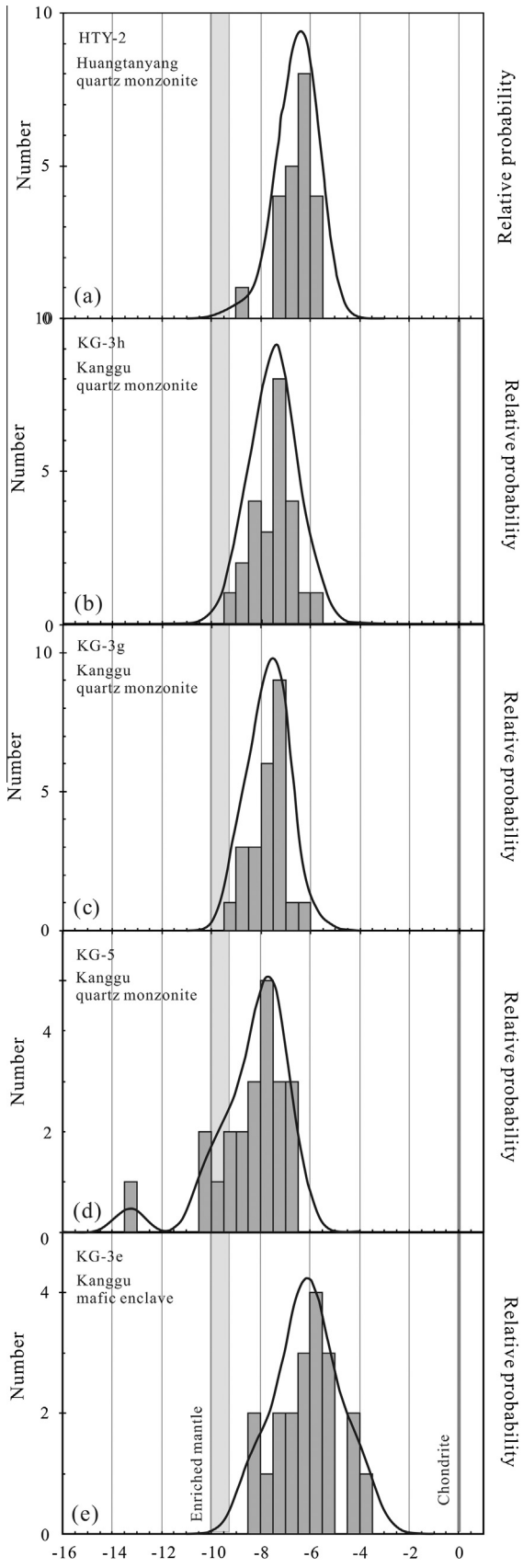

Fig. 10. Histograms of zircon $\varepsilon_{Hf}(t)$ values of Huangtanyang and Kanggu plutons.

that were initially quenched and then crystallised in the host felsic magma. For example, the MMEs have igneous mineral assemblages and textural evidence for disequilibrium, such as acicular apatite and plagioclase with complex oscillatory zoning and repeated resorption surfaces (Fig. 3f). These are interpreted as being indicative of chemical and/or thermal changes in the melt during crystal growth, potentially as a result of magma mixing (Baxter and Feely, 2002; Grogan and Reavy, 2002). Secondly, zircon morphology and Hf isotopic data presented here places even more robust qualitative constraints on the origin of MMEs. As a mineral crystallized in the early of magma, zircon has high Lu–Hf closure temperature and hence can record primitive and subsequent isotopic signatures of the magmatic component during the mixing process (Andersen et al., 2007; Belousova et al., 2006; Chen et al., 2009; Griffin et al., 2002; Li et al., 2009; Yang et al., 2007; Zhao et al., 2012). Zircons from the Kanggu quartz monzonites have the same crystallization ages as those from the MMEs, but they exhibit different morphology and $\varepsilon_{Hf}(t)$ values (Figs. 10 and 11). The morphology of zircon populations from the host quartz monzonite and enclaves could reveal the differences in their crystallisation conditions (e.g., Pupin, 1980; Wang, 1998; Wang and Kienast, 1999; Belousova et al., 2002). Zircon crystals from the host quartz monzonites are elongate prisms and exhibit regular magmatic oscillatory zoning in CL images, whereas most zircon grains from the MMEs are stubby and show absorption zoning in CL images, which indicates an origin from mafic magma. Furthermore, the enclave samples have relatively depleted zircon Hf isotopic compositions with higher $\varepsilon_{Hf}(t)$ values varying from −8.4 to −3.8, whereas the host quartz monzonites have highly variable zircon Hf isotopic compositions with $\varepsilon_{Hf}(t)$ values varying from −13.3 to −5.8 (Fig. 10). The difference in zircon $\varepsilon_{Hf}(t)$ values between the MMEs and host rocks, together with the wide range in zircon Hf isotopic compositions provides the most direct evidence for mixing between mafic and felsic magmas from different sources (e.g., Yang et al., 2006, 2007; Zhao et al., 2012). Meanwhile, some zircons (e.g., KG-3e-4) in the enclaves have similar CL patterns, U–Pb ages, and Hf isotopic compositions to those in the host rocks and, as stated previously, many MMEs contain feldspar and quartz megacrysts that were entrained from the host granites. These observations further support the inference that magma mixing/mingling occurred during the genesis of the MMEs (e.g., Griffin et al., 2002).

It is worth noting that when a more mafic magma is injected into a felsic magma chamber and then breaks up into globular enclaves, both magma mingling and chemical diffusion act to modify the original composition of the enclave magma. The mafic enclaves are characterised by higher contents of hydrous minerals (hornblende and biotite) than their host rocks, strongly suggests that the migration of fluids from the host felsic magma to enclaves was effective (Wiebe, 1973; Orsini et al., 1991; Blundy and Sparks, 1992). During the processes of fluid influx, chemical transfer of some mobile elements would be inevitable. As such, we speculate that the similar trace element and Sr–Nd isotopic compositions of the MMEs and host quartz monzonites were caused by diffusion and partial re-equilibration, as a natural consequence of the mixing/mingling model (e.g., Xiong et al., 2011; Zhao et al., 2012; Liu et al., 2013).

5.2. Petrogenesis of quartz monzonites

There are several hypotheses proposed for the origins of monzonite magmas, including: (1) partial melting of crustal rocks (Xu et al., 2004; Köksal et al., 2013); (2) fractional crystallization from

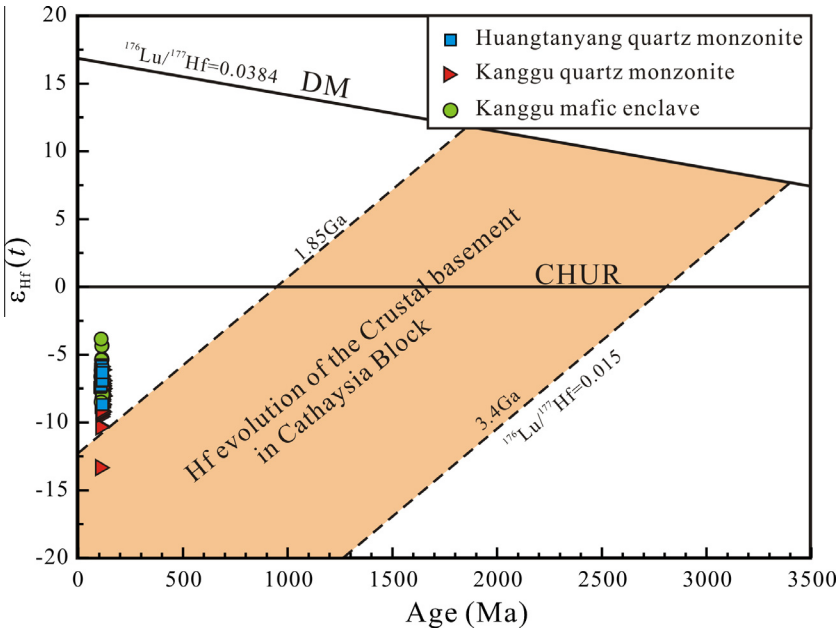

Fig. 11. $\varepsilon_{Hf}(t)$ *vs.* U–Pb ages for zircons from the Huangtanyang and Kanggu plutons. The values used for constructing the depleted mantle (DM) and crustal evolution reference lines were taken from Griffin et al. (2000, 2002). The Hf evolutionary area shown for the crustal basement of the Cathaysia Block is from Xu et al. (2007).

mantle-derived basaltic magmas with or without crustal assimilation (Rapela and Pankhurst, 1996; Jiang et al., 2002; Wang et al., 2007; Liu et al., 2008; Li et al., 2009; Aghazadeh et al., 2010, 2011); and (3) magma mixing between mantle-derived mafic and crustally derived silicic magmas (Neves and Mariano, 1997; Ferré et al., 1998; Yaliniz et al., 1999; Gagnevin et al., 2004; Ackerman et al., 2010; Yang et al., 2011; Lan et al., 2011, 2012, 2013; Cheng et al., 2012; Donskaya et al., 2013; Mao et al., 2013; Wang et al., 2013; Liu et al., 2013, 2014b). Both the Huangtanyang and the Kanggu quartz monzonites possess similar geochemical features, such as similar zircon U–Pb ages, major elements and Sr–Nd–Hf isotopic compositions, suggesting that they were derived from similar sources and generated by similar petrogenetic processes, therefore in the following sections we will discuss their petrogenesis together.

5.2.1. Crustal contamination and crystal fractionation

The Huangtanyang and the Kanggu quartz monzonites have relatively constant Sr–Nd isotopic compositions over the SiO_2, which could argue against crust assimilation-fractional crystallisation (AFC) processes and may reflect a simple fractionation crystallization (FC) process. However, the negative correlation of SiO_2 vs. Al_2O_3 (Fig. 12a) in the monzonites requires the fractionation of plagioclase and/ or K-feldspar if FC occurs. This process would decrease Na_2O and/or K_2O with increasing SiO_2 in these quartz monzonites, and would also result in significant Eu anomalies, which is contrary to what is actually observed (Fig. 12b–d).

The constant Ni and Cr contents with increasing Zr concentrations suggest that the fractionation of pyroxene was negligible during magma evolution of the Huangtanyang and the Kanggu quartz monzonites. The observed high Zr and Hf contents and marked positive Zr and Hf anomalies (Fig. 8b) preclude titanite and/or rutile FC in the parental magmas, because either titanite or rutile FC wound not only yield negative anomalies in Nb, Ta, and Ti but also lead to depletion of Zr and Hf (Klemme et al., 2005). Therefore, the characteristics of Nb, Ta and Ti depletion are likely to be intrinsic to their parental magma sources. Insignificantly negative Eu or Sr anomalies indicate that feldspar (plagioclase or K-feldspar) could not have been a major fractionating phase. Meanwhile, δEu values remain constant with increasing SiO_2 (Fig. 12d) and decreasing CaO (not shown), which also suggests that fractionation of plagioclase was negligible. It is worth noting that all quartz monzonites have relatively low differentiation index (D.I. = 71.5–79.9; Table 1). Collectively, we thus suggest only a subordinate role of FC during magmatic evolution of Huangtanyang and Kanggu quartz monzonites.

5.2.2. Potential magma sources

As discussed above, the effects of fractional crystallisation (FC) or crustal assimilation are most likely negligible in the formation of the Huangtanyang and the Kanggu quartz monzonites. Meanwhile, the SiO_2 contents of the quartz monzonites from the both plutons are relatively high (61.35–66.22 wt.%) to represent magmas derived by direct partial melting of the mantle, as the latter cannot yield melts more silicic than andesitic compositions with <57% SiO_2 (Lloyd et al., 1985; Baker et al., 1995). Therefore, the crustal materials must have been involved in the formation of the Huangtanyang and the Kanggu quartz monzonites. Furthermore, the existence of some zircons with unusually low $\varepsilon_{Hf}(t)$ values (low to −13.3) and Palaeoproterozoic two-stage Hf model ages (T_{DM2} (Hf); up to 1.97 Ga) from the Huangtanyang and the Kanggu quartz monzonites argues strongly for Palaeoproterozoic crustal involvement (Griffin et al., 2000; Xu et al., 2007).

On the other hand, elemental and isotopic data also support that a significant amount of mantle-derived component was involved in their magma genesis. Firstly, Rapp and Watson (1995) have proposed that melts from the basaltic lower continental crust are characterised by low Mg# values (<40) regardless the degree of melting, whereas those with higher Mg# values (>40) can only be generated by involvement a mantle component. In this study, both the Huangtanyang and the Kanggu quartz monzonites have higher Mg# values than those generated solely by partial melting of crustal materials (Fig. 13), implying the input of mantle-derived components (e.g., Jiang et al., 2013). Secondly, a majority of zircons from the Huangtanyang and the Kanggu quartz monzonites plot above the isotope evolution field for crustal basement of the Cathaysia Block (Fig. 11), and two-stage Hf model ages of most zircons (1.50–1.69 Ga for the Huangtanyang and

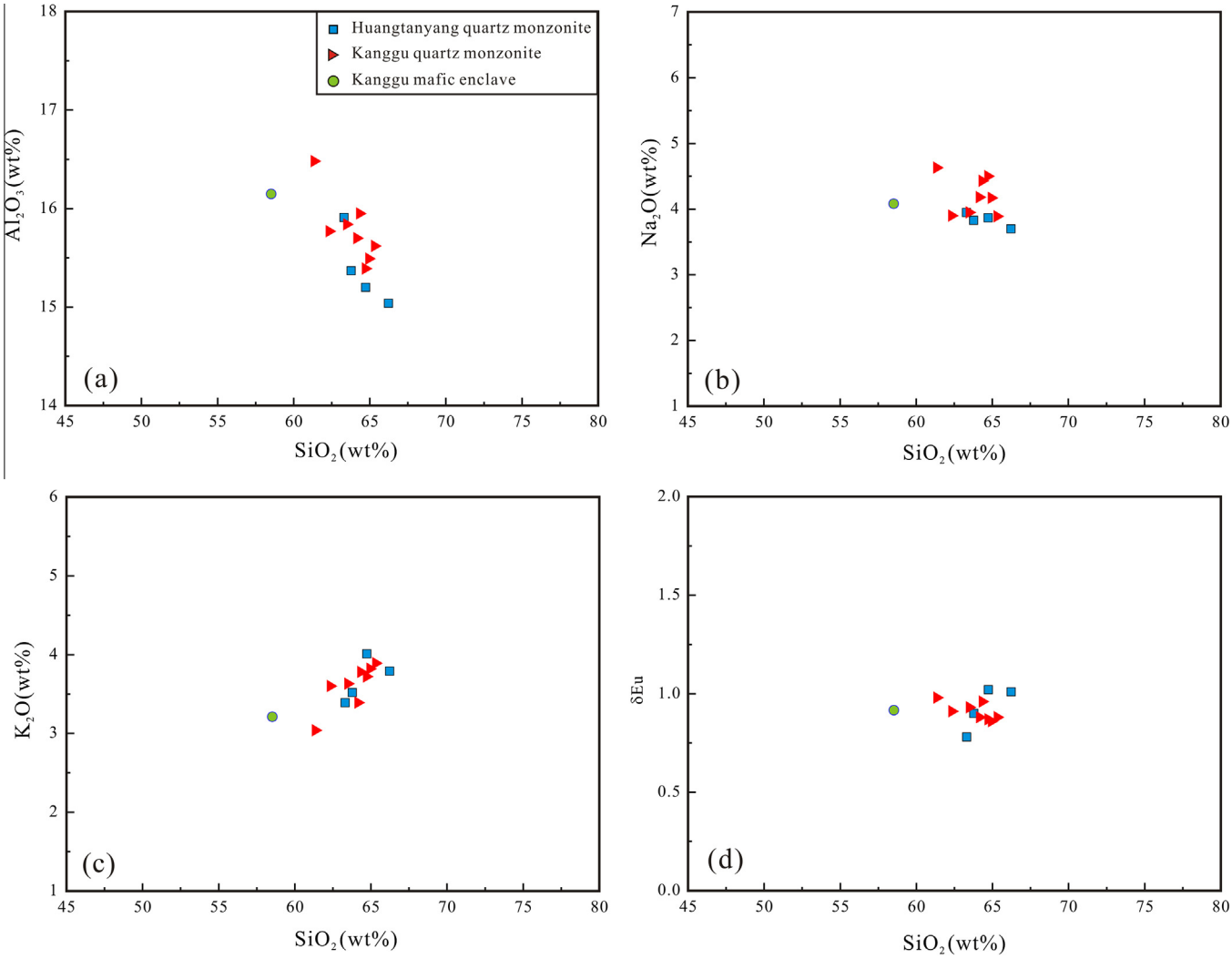

Fig. 12. SiO_2 vs. major element oxides and Sr–Nd isotopes for the Huangtanyang and Kanggu plutons.

1.51–1.97 Ga for the Kanggu quartz monzonites) are younger than that of the basement (>1.85 Ga; Xu et al., 2007). Moreover, Yu et al. (2010) suggested that there were five important episodes of juvenile crust generation (3.6 Ga, 2.8 Ga, 2.6–2.4 Ga, 1.85 Ga, and 0.8–0.7 Ga) in this area. The majority of zircon Hf model ages are inconsistent with any proposed episode of regional crust generation, thus indicating mantle components have been involved in their genesis.

Nb/U or Ta/U ratios are useful indexs for discriminating magma sources, because these values are not significantly affected by variable degrees of partial melting or subsequent fractional crystallization (Hofmann, 1988; Xu et al., 2005; Ma et al., 2014). Nb/U ratios from the Huangtanyang and the Kanggu quartz monzonites (Nb/U = 2.2–4.1) are significantly lower than those of mid-ocean ridge and ocean island basalts (MORB and OIB, Nb/U ≈ 47; Hofmann et al., 1986) and the lower crust (Nb/U ≈ 25; Rudnick and Gao, 2003), and are even lower than the mean value of upper crust (Nb/U ≈ 4.5; Rudnick and Gao, 2003), implying that such signatures cannot be solely generated by melting of continental crust or depleted mantle. Noteworthily, as the HFSEs are likely to be stored in residual rutile and ilmenite in the subducted slab, fluids dehydrated from a subducted slab could have very low Nb/U ratios (~0.22) that reflect the transfer of significant amounts of LILEs into the slab-derived fluids (Ryerson and Watson, 1987; Ayers, 1998). The Huangtanyang and the Kanggu quartz monzonites are characterised by strong fractionation between LREE and HREE, enrichment of LILEs, and depletion of HFSEs with negative Ta, Nb, and Ti anomalies. These characteristics are similar to those of the contemporary Cretaceous mafic suites in the Cathaysia Block which are widely considered to be derived from a metasomatized mantle source (Chen et al., 2008; Meng et al., 2012; Li and Jiang, 2014a,b). Li et al. (1997) advocated that the lithospheric mantle beneath SE China was modified by an ancient, recycled, subducted plate during the Mesozoic. Therefore, we argue that the very low Nb/U ratios of the Huangtanyang and the Kanggu quartz monzonites were likely inherited from lithospheric mantle metasomatised by fluids released from a dehydrating slab during a past subduction event. The relatively low Ta/U ratios of the Huangtanyang and the Kanggu plutons (0.17–0.28) also favour this hypothesis.

Most quartz monzonites samples from the Huangtanyang and the Kanggu plutons have higher and constant K_2O contents than those typically observed in the continental upper crust (3.4 wt.%; Taylor and McLennan, 1985), suggesting a potassic phase such as phlogopite, potassic amphibole or K-feldspar in the source region. The positive correlation between the La concentrations and La/K ratios (not shown) further supports that a potassic phase of phlogopite or potassic amphibole is present in the magma source

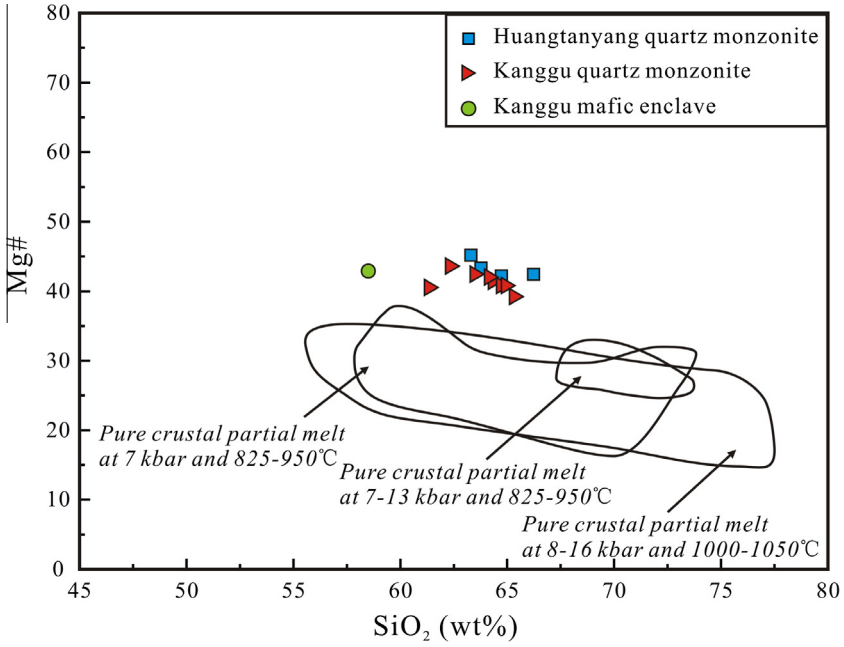

Fig. 13. Mg# vs. SiO_2 diagram for the Huangtanyang and Kanggu plutons. Also shown are the fields of pure crustal partial melts determined in experimental studies on dehydration melting of low-K basaltic rocks at 8–16 kbar and 1000–1050 °C (Rapp and Watson, 1995), of moderately hydrous (1.7–2.3 wt.% H_2O) medium- to high-K basaltic rocks at 7 kbar and 825–950 °C (Sisson et al., 2005), and of pelitic rocks at 7–13 kbar and 825–950 °C (Patiño Douce and Johnston, 1991).

region. However, the absence of significant Eu anomalies of these rocks (Fig. 8a) suggests a K-feldspar-free source. Meanwhile, the rocks have significantly high Rb/Sr (0.16–0.43) and low Ba/Rb (5.37–10.16) ratios, similar to those of the melts in equilibrium with phlogopite (Rb/Sr > 0.1, Ba/Rb < 20), but different from those of amphibole-bearing mantle sources (Rb/Sr < 0.06, Ba/Rb > 20, respectively), strongly suggesting phlogopite rather than potassic amphibole as the main potassic phase (Feldstein and Lange, 1999). The presence of phlogopite in the source region is consistent with the metasomatized mantle, in which phlogopite is a common metasomatic volatile-bearing phase (e.g., Ionov et al., 1997). Fluid metasomatism or melt hybridization would involve the formation of phlogopite in the lithospheric mantle. The quartz monzonites from Huangtanyang and the Kanggu plutons are enriched in LILE (e.g., Ba = 1021–1343 ppm; Sr = 442–735 ppm) (Fig. 8b), at concentrations that are higher than those in the continental crust (Ba = 390 ppm and Sr = 350 ppm; Rudnick and Fountain, 1995). It has been suggested that metasomatic volatile-bearing phases (phlogopite or amphibole) are the major repositories for LILE in the lithospheric mantle (e.g., Ionov et al., 1997), and thus could account for such an enrichment. Nevertheless, as suggested by Wang et al. (2005, 2008) and He et al. (2010), the subcontinental lithospheric mantle of South China is isotopically of EM-II type, and can be represented by the Yangfang aegirine–augite syenite in western Fujian (Fig. 9). Most zircons from the Huangtanyang and the Kanggu quartz monzonites have higher $\varepsilon_{Hf}(t)$ (up to −5.7) than average values for enriched mantle (approximately −10.3, Fig. 10; He et al., 2010), which also provides evidence for participation of some depleted mantle components in their petrogenesis. Recent studies with systematic Nd–Hf isotope analyses also show that melts from a depleted mantle source have been involved during the generation of some Late Yanshanian rocks along the Zhejiang and Fujian coastal area (He and Xu, 2012; Liu et al., 2014b; Z. Li et al., 2014).

From another point of view, the La/Nb ratios and Sr–Nd isotopes can also help to elucidate secular changes in the mantle source region (e.g., Meng et al., 2012), and here support that both depleted and metasomatically enriched mantle components were involved in the petrogenesis of Huangtanyang and the Kanggu quartz monzonites. The quartz monzonite samples (HTY-2 or HTY-3) from Huangtanyang plutons have the lowest La/Nb ratios (1.6–1.8), suggesting a subcontinental lithosphere mantle-origin with a small contribution from the asthenosphere (Fig. 14). The majority of the Huangtanyang and the Kanggu quartz monzonites have elevated La/Nb ratios (3.2–8.5) which deviate significantly from this asthenosphere–lithosphere mantle mixing trend (Fig. 14). The overall heterogeneity is explained either by involvement of crustal materials or a subduction component. Considering that their La/Nb ratios are much higher than those in the continental crust (~3.8; Rudnick and Gao, 2003), a subduction component is required for their magma sources. In fact, the coeval basaltic rocks in the coastal region of Cathaysia Block show similar characteristics (Figs. 8 and 15), which were suggested to be mixing products between mantle melts and a subduction-related component (Chen et al., 2008; Meng et al., 2012). Meng et al. (2012) also suggest that such characteristic can be generated by partial melting of subcontinental lithosphere mantle (SCLM) at the base of lithosphere that was metasomatised by slab-induced melts and fluids. In addition, MMEs from the Kanggu pluton have higher La/Nb ratios (La/Nb = 5.4) and Sr concentrations (790 ppm) than their host quartz monzonites (La/Nb = 3.4–4.4; Sr = 526–735 ppm), implying more enriched lithospheric mantle components had been involved.

5.2.3. A hybrid origin

Consequently, we conclude that both mantle components (i.e., depleted and metasomatically enriched mantle) and Palaeoproterozoic crustal materials were involved in the formation of the Huangtanyang and the Kanggu quartz monzonites. It is important to note that Nb/Ta ratios of the Huangtanyang and the Kanggu quartz monzonites vary from 13.0 to 15.6, which fall in the range of those for continental crust (12–13; Barth et al., 2000), MORB (16.7 ± 1.8; Kamber and Collerson, 2000), and primitive mantle (17.5 ± 2.0; Green, 1995; Sun and McDonough, 1989). Moreover, the Hf–Nd isotopic compositions of the Huangtanyang and Kanggu quartz monzonites are intermediate between those of depleted mantle and crustal basement (Figs. 9 and 10). These features

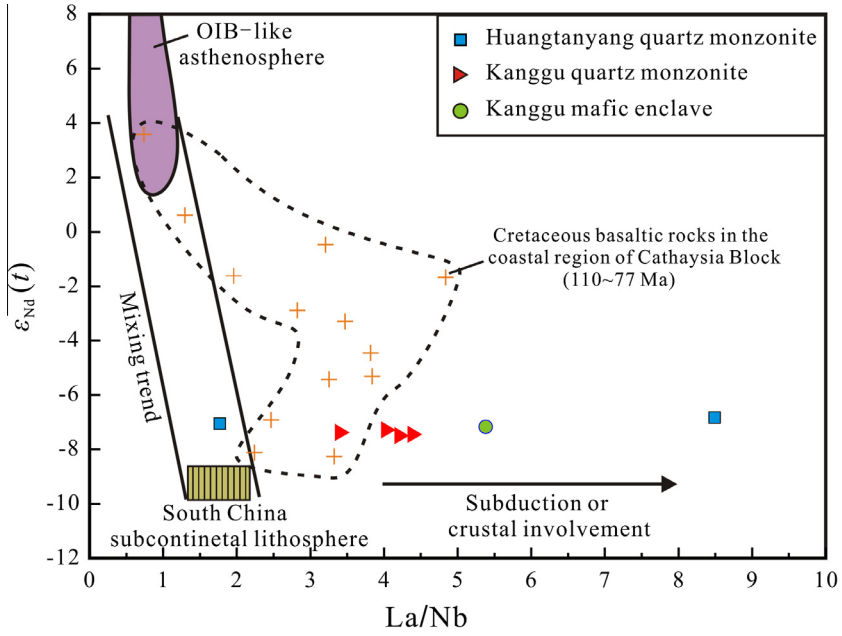

Fig. 14. $\varepsilon_{Nd}(t)$ vs. La/Nb diagram for the Huangtanyang and Kanggu plutons. The OIB-asthenosphere and South China subcontinental lithosphere are after Chen et al. (2008). The values for the Cretaceous basaltic rocks in the coastal region of Cathaysia Block are from Meng et al. (2012).

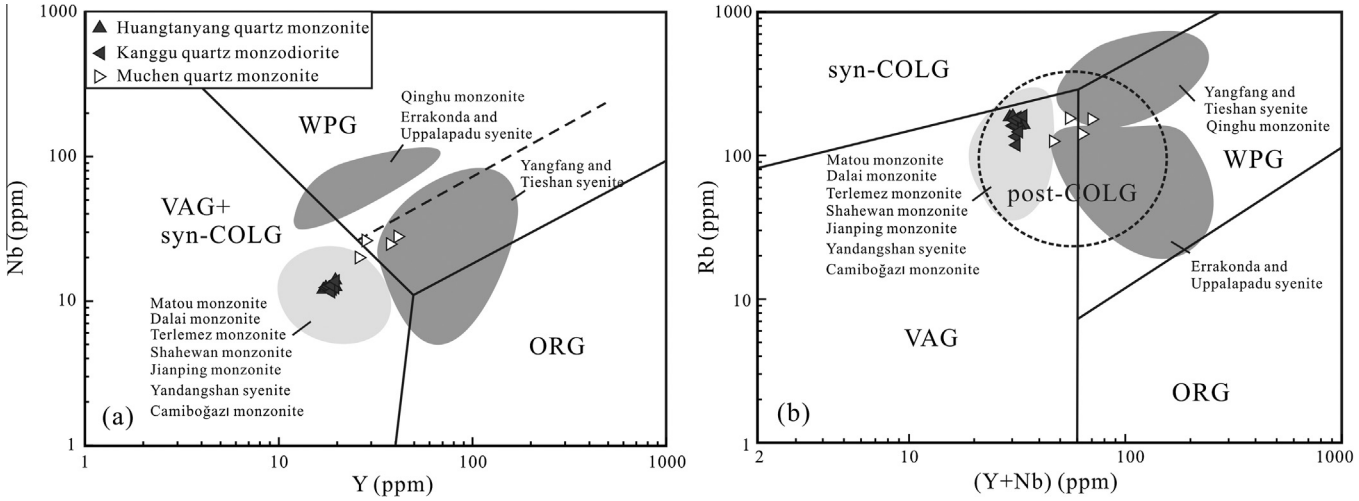

Fig. 15. Tectonic discrimination diagrams of Pearce et al. (1984) and Pearce (1996) showing the possible tectonic setting for the Kanggu and Huangtanyang plutons. Also shown are the fields for the Yangfang and Tieshan syenites (Wang et al., 2005), Errakonda and Uppalapadu syenites (Kumar et al., 2007), Qinghu monzonite (Li et al., 2004), Terlemez monzonite (Yaliniz et al., 1999), Muchen monzonite (Liu et al., 2013), Matou and Dalai monzonites from (Liu et al., 2014b), Shahewan monzonite (Wang et al., 2007), Yandangshan syenite (He et al., 2009), Camiboğazı monzonite (Kaygusuz et al., 2014), and Jianping monzonite (W. Wang et al., 2013). Abbreviations: WPG: within-plate granites; VAG: volcanic arc granites; syn-COLG: syn-collision granites; ORG: Oceanic ridge granites; post-COLG: post-collision granites.

suggest that the Huangtanyang and Kanggu quartz monzonites formed from mixing between mantle-derived basaltic magmas and ancient crust-derived melts. The following two lines of evidence also favour this interpretation:

(1) Abundant MMEs from the Huangtanyang and Kanggu pluton are considered to be globules of near-liquidus mafic melt that was injected into and mingled with the host felsic magma.
(2) The quartz monzonites exhibit a wide range of zircon Hf compositions with a multi-peak distribution (Fig. 10), especially for the Kanggu plutons, which precludes a simple, cogenetic evolution via closed-system fractionation and necessitates a magma mixing model (e.g., Yang et al., 2006, 2007; Zhao et al., 2012; Liu et al., 2013, 2014b).

5.3. Record evidence for crust–mantle interaction

As discussed above, the Huangtanyang and Kanggu quartz monzonites were derived from mixing between mantle-derived basaltic magmas and ancient crust-derived melts. Magma mixing has been extensively indicated by evidence from several Cretaceous intrusions in SE China, such as the occurrence of hybrid origin enclaves from Muchen quartz monzonite (Liu et al., 2013), Matou quartz monzonites (Liu et al., 2014b), Putuoshan granite (Xie et al., 2004; X.L. Zhang et al., 2005), Xiaojiang granite (Hsieh et al., 2009; Wang et al., 2013), and Pingtan granite (Griffin et al., 2002), and by mingling structures in the Pingtan igneous complex (Dong et al., 1998; Xu et al., 1999).

To estimate the proportions of mantle and crustal components involved in the genesis of the quartz monzonites during this study, we used a mixing model similar as Liu et al. (2014b). A typical Qinghu monzonite was selected to represent the depleted mantle end-member, as this monzonite has the most radiogenic Sr, Nd, and Hf isotope compositions recorded to-date for Mesozoic igneous rocks in south China (Chen and Jahn, 1998; Li et al., 2004, 2009). We used a typical Darongshan S-type granite from Guangxi Province to represent the crustal end-member, as it is thought to have formed by remelting of purely silicic crust (Hsieh et al., 2008). The Yangfang aegirine–augite syenite from western Fujian Province was selected to represent the enriched lithospheric mantle end-member (Wang et al., 2005). Our calculations show that the Huangtanyang and Kanggu quartz monzodiorites can be modelled isotopically by mixing 30–33% of depleted mantle melts and 67–70% of enriched mantle melts, or mixing 43–49% of depleted mantle melts and 51–57% of crustal melts. Thus, a proportion of 30–49% of depleted mantle melts is required for the formation of the Huangtanyang and Kanggu quartz monzonites, which is less than that involved in formation of the Muchen quartz monzonite, Matou quartz monzonite and Dalai quartz monzodiorite in western Zhejiang Province (Fig. 9; Liu et al., 2013, 2014b). The Late Mesozoic crust–mantle interaction in SE China has been also widely recognised by previous studies, with an increasing contribution of contemporaneous underplated hot mantle-derived magmas as both a heat source inducing crustal melting and a source of materials that variably mixed with the local crustal melts (e.g., Xue et al., 1996; Chen and Jahn, 1998; Xu et al., 1999; Guo et al., 2012; L. Liu et al., 2012; Hong et al., 2013; Liu et al., 2013, 2014a; Z. Li et al., 2014), suggesting that these magmatic activities were controlled by a common geodynamic mechanism rather than independent tectonic events.

The geodynamic mechanism of the widespread Late Mesozoic magmatic rocks in SE China have become an important topic of international research interest (Zhao et al., 2015). Despite some controversy, a growing number of researchers consider that Cretaceous magmatism along the coastal area of SE China was formed in an active continental margin due to subduction of the Palaeo-Pacific plate beneath the Eurasian continent (Zhou et al., 2006; X.H. Li et al., 2007; Li and Li, 2007; Chen et al., 2008).

In this study, we also recognise the involvement of mafic melts from both depleted and enriched mantle during this magmatism. The involvement of mafic melts from both depleted and enriched mantle during magmatism leads us to suggest an upwelling of the asthenospheric mantle. The asthenosphere-derived magma can cause small degrees of partial melting of phlogopite-bearing lithospheric mantle which could resulted in the generation of the mafic magma for Huangtanyang and Kanggu quartz monzonite. However, the asthenosphere is unlikely to melt significantly on decompression unless it rises to depths less than 50 km (Atherton and Ghani, 2002), which may need the extension of lithospheric beneath SE China. Actually, the thinning of the lithospheric mantle from the Palaeozoic to the Cenozoic in SE China had been supported by Xu et al. (2000), and they proposed that at least 100 km of Archaean to Proterozoic lithospheric mantle has been removed since Late Mesozoic times. In fact, the extension-related igneous rocks, mainly in the coastal SCB, include bimodal volcanic rocks, A-type granites, aplites and diabase dikes (Dong et al., 1997, 2006; Wang, 2002; Qiu et al., 2004, 2008; Chen et al., 2008, 2013; Zhao et al., 2015), accompanied with a series of pull-apart basins (Xing et al., 2009; Zhou et al., 2006), strongly suggest that SE China was in an extensional setting during Cretaceous times. What's more, it has been suggested that the timing of the transition from a compressional subduction regime to an extensional regime in SE China occurred at ca. 110 Ma (Tao et al., 2000; He and Xu, 2012). The Huangtanyang and Kanggu plutons are located in the coastal area of SE China and formed in the Cretaceous (104–109 Ma), which corresponds to the extensional regime. In the Nb–Y or Rb–(Y + Nb) tectonic discrimination diagram proposed by Pearce et al. (1984), data for all samples from these plutons plot in the VAG (volcanic arc granites) field (Fig. 15). Furthermore, all samples plot in the post-collisional granite (post-COLG) field on Rb–(Y + Nb) diagram (Fig. 15b; Pearce, 1996), as do data for several other monzonitic or syenitic plutons (e.g., the Terlemez, Muchen, Shahewan, Jianping and Camiboğazı monzonites), which are interpreted to have formed in a post-collisional extensional setting (Yaliniz et al., 1999; Wang et al., 2007, 2013; Liu et al., 2013, 2014b; Kaygusuz et al., 2014). In comparison, the Qinghu monzonite (Li et al., 2004), the Errakonda and Uppalapadu syenites (Kumar et al., 2007), and the Yangfang and Tieshan syenites (Wang et al., 2005), which formed in intra-continental extensional environments, plot in the WPG (within-plate granite) field in Fig. 15. Consequently, both the Huangtanyang and Kanggu quartz monzonites were most likely generated in a post-collisional extensional tectonic setting. In contrast, the Muchen pluton was emplaced at 112 Ma, with samples plotting in both the VAG and WPG field, which corresponds to the tectonic transition period from compression to extension (Liu et al., 2013).

Lithospheric extension can be caused in a various ways. The Mesozoic lithospheric extension in SE China was previously considered to be related to rollback and delamination of the subducted Paleo-Pacific slab (Li and Li, 2007; Wong et al., 2009), southwestward ridge subduction (e.g., Ling et al., 2009; Sun et al., 2007) or oblique subduction of the Pale-Pacific Ocean (Wang et al., 2011). A back-arc extension has also been proposed to explain the Mesozoic A-type granitic magmatism in SE China (e.g., Wong et al., 2009). All these processes could trigger decompression melting of the mantle reservoirs and underplating of hot mantle-derived magmas in the crust. Based on systematical researches on the Cretaceous volcanic rocks and a series of granitoid plutons in Zhejiang, Liu et al. (2014a) identified that the juvenile component involvement gradually occurred from the inland to the coast under an enhanced lithospheric extensional tectonic setting. Note this migration and the enhance of lithospheric extension, an increasing dip angle of the subducted slab, i.e. slab rollback, is suggested to account for the Cretaceous geodynamics in the area, since the slab rollback would consequently have led to the retreat of the trench oceanward and generated the back-arc extensional environment (Stern, 2002).

Accordingly, we propose a simplified genetic model for the Huangtanyang and Kanggu quartz monzonites, which is summarised as follows: (1) as the dip angle of the subducted slab increased and the trench retreated oceanward, the lithosphere was thinned by extension; (2) this resulted in asthenospheric upwelling and melting which transferred energy and magma into the continental lithosphere, and; (3) this then triggered partial melting of the enriched lithospheric mantle. Asthenospheric melts mixed with enriched lithospheric mantle melts thus generated the primary mantle magmas of the Huangtanyang and Kanggu plutons. At the same time, larger amounts of basaltic magma derived from variable amounts of mixing between melts of asthenospheric and enriched lithospheric mantle ascended to the base of the lower crust and triggered partial melting of crustal materials. Crust-derived melts then mixed with the basaltic magmas, forming the Huangtanyang and Kanggu quartz monzonitic magma. Sparks et al. (1977) mentioned that magma is quickly superheated when mixed with mafic magma resulting in increased temperature producing a significant lowering of its viscosity. If mafic magma is introduced before of crystallization of the felsic magma, it may result in homogeneous hybrid magmas. This type of mixing often occurs at depth and is usually favoured by convection. However,

if it is introduced slightly later, then the viscosities of two magmas may be sufficiently contrasting to only allow mingling. The mafic magma may also break up into blobs and can be scattered in the felsic magma to form enclaves. Therefore, injection of successive pulses of mafic magma into the ascending monzonitic magma would have formed the MMEs in this study (e.g., Fernandez and Barbarin, 1991). The calculated zircon saturation temperatures (t_{Zr}) of Huangtanyang and Kanggu quartz monzonites are in the range of 793–804 °C and 799–831 °C (Table 2; Watson and Harrison, 1983), indicating generation for both plutons at relatively high temperatures, which is consistent with the above interpretation. What's more, previous studies show that there may be a 4–5 km thick mafic magma layer storing in the middle and lower crust of SE China (Li and van der Hilst, 2010; Xu et al., 1996, 1999; Zhang and Wang, 2007; Zhang et al., 2008; Liu et al., 2014a), which could offer the channel for mixing between components of asthenospheric and enriched lithospheric mantle.

6. Conclusions

The following conclusions can be reached based on the comprehensive petrological, geochemical, and Sr–Nd–Hf isotopic investigation of the Huangtanyang and Kanggu quartz monzonites in eastern Zhejiang Province, SE China:

(1) LA-ICP-MS zircon U–Pb dating results imply that the Huangtanyang and Kanggu quartz monzonites were emplaced in Cretaceous (104–109 Ma), whereas MMEs from Huangtanyang crystallised at 109.9 ± 1.1 Ma, and are coeval with their host monzonites (109.0 ± 1.4 Ma).
(2) Abundant petrological and microstructural observations, and zircon Hf isotopic data indicate that the MMEs were globules of mafic magma that were initially quenched and then crystallised in the host felsic magma.
(3) Whole-rock chemical and isotopic data and zircon Hf isotopic compositions support that the Huangtanyang and Kanggu quartz monzonites were derived from mixing between mantle-derived basaltic magmas and ancient crust-derived melts under an extensional regime.

Acknowledgments

We thank Prof. Antonio Castro, Prof. Boris Litvinovsky, and an anonymous reviewers for their thoughtful comments and constructive suggestions which greatly improved the manuscript. We also thank Ms. Y.L. Li for assisting us in data collection, and Ms. W. Pu for her assistance with Sr–Nd isotope analysis. This study was financially supported by the Natural Science Foundation of China (Grant No. 41272084), the National 973 Project of the Chinese Ministry of Science and Technology (Grant No. 2012CB416702), and the Specialized Research Fund for the Doctoral Program of Higher Education of China (Grant No. 20120091130003).

Appendix A. Supplementary material

Supplementary data associated with this article can be found, in the online version, at http://dx.doi.org/10.1016/j.jseaes.2015.09.022.

References

Ackerman, L., Krňanská, M., Siebel, W., Strnad, L., 2010. Geochemistry of the Drahotín and Mutěnín intrusions, West Bohemian shear zone, Bohemian massif: contrasting evolution of mantle-derived melts. Mineral. Petrol. 99, 185–199.
Aghazadeh, M., Castro, A., Omran, N.R., Emami, M.H., Moinvaziri, H., Badrzadeh, Z., 2010. The gabbro (shoshonitic)–monzonite–granodiorite association of Khankandi pluton, Alborz Mountains, NW Iran. J. Asian Earth Sci. 38, 199–219.
Aghazadeh, M., Castro, A., Badrzadeh, Z., Vogt, K., 2011. Post-collisional polycyclic plutonism from the Zagros hinterland. The Shaivar-Dagh plutonic complex Alborz belt, Iran. Geol. Mag. 148, 980–1008.
Andersen, T., 2002. Correction of common lead in U–Pb analyses that do not report 204Pb. Chem. Geol. 192, 59–79.
Andersen, T., Griffin, W.L., Sylvester, A.G., 2007. Sveconorwegian crustal underplating in southwestern Fennoscandia: LAM-ICPMS U–Pb and Lu–Hf isotope evidence from granites and gneisses in Telemark, southern Norway. Lithos 93, 273–287.
Atherton, M.P., Ghani, A.A., 2002. Slab breakoff: a model for Caledonian, Late Granite syncollisional magmatism in the orthotectonic (metamorphic) zone of Scotland and Donegal, Ireland. Lithos 62, 65–85.
Ayers, J., 1998. Trace element modeling of aqueous fluid–peridotite interaction in the mantle wedge of subduction zones. Contrib. Miner. Petrol. 132, 390–404.
Baker, M.B., Hirschmann, M.M., Ohiorso, M.S., Stolper, E.M., 1995. Compositions of near-solidus peridotite melts from experiments and thermodynamic calculations. Nature 375, 308–311.
Barth, M.G., McDonough, W.F., Rudnick, R.L., 2000. Tracking the budget of Nb and Ta in the continental crust. Chem. Geol. 165, 197–213.
Baxter, S., Feely, M., 2002. Magma mixing and mingling textures in granitoids: examples from the Galway Granite, Connemara, Ireland. Mineral. Petrol. 76 (1–2), 63–74.
Barbarin, B., 2005. Mafic magmatic enclaves and mafic rocks associated with some granitoids of the central Sierra Nevada batholith, California: nature, origin, and relations with the hosts. Lithos 80, 155–177.
Belousova, E.A., Griffin, W.L., O'reilly, S.Y., Fisher, N.I., 2002. Igneous zircon: trace element composition as an indicator of source rock type. Contrib. Miner. Petrol. 143, 602–622.
Belousova, E.A., Griffin, W.L., O'Reilly, S.Y., 2006. Zircon crystal morphology, trace element signatures and Hf isotope composition as a tool for petrogenetic modelling: examples from Eastern Australian granitoids. J. Petrol. 47 (2), 329–353.
Black, L.P., Gulson, B.L., 1978. The age of the mud tank carbonatite, Strangways range, Northern territory. BMR J. Aust. Geol. Geophys. 3, 227–232.
Blundy, J.D., Sparks, R.S.J., 1992. Petrogenesis of mafic inclusions in granitoids of the Adamello Massif, Italy. J. Petrol. 33, 1039–1104.
Bouvier, A., Vervoort, J.D., Patchett, P.J., 2008. The Lu–Hf and Sm–Nd isotopic composition of CHUR: constraints from unequilibrated chondrites and implications for the bulk composition of terrestrial planets. Earth Planet. Sci. Lett. 273, 48–57.
Boynton, W.V., 1984. Geochemistry of the rare earth elements: meteorite studies. In: Henderson, P. (Ed.), Rare Earth Elements Geochemistry. Elsevier, Amsterdam, pp. 63–144.
Castro, A., Aghazadeh, M., Badrzadeh, Z., Chichorro, M., 2013. Late Eocene–Oligocene post-collisional monzonitic intrusions from the Alborz magmatic belt, NW Iran. An example of monzonite magma generation from a metasomatized mantle source. Lithos 180–181, 109–127.
Chappell, B.W., White, A.J.R., 1974. Two contrasting granite types. Pacific Geol. 8, 173–174.
Chappell, B.W., White, A.J.R., Wyborn, D., 1987. The importance of residual source material restite in granite petrogenesis. J. Petrol. 28, 1111–1138.
Chappell, B.W., White, A.J.R., 1992. I- and S-types granites in the Lachland Fold Belt. Trans. R. Soc. Edinburgh: Earth Sci. 83, 1–26.
Chappell, B.W., White, A.J.R., Williams, I.S., Wyborn, D., Wyborn, L.A.I., 2000. Lachlan Fold Belt granites revisited: high- and lowtemperature granites and their implications. Aust. J. Earth Sci. 47, 123–138.
Chen, B., Chen, Z.C., Jahn, B.M., 2009. Origin of mafic enclaves from the Taihang Mesozoic orogen, north China craton. Lithos 110 (1–4), 343–358.
Chen, C.H., Lee, C.Y., Shinjo, R., 2008. Was there Jurassic paleo-Pacific subduction in South China?: constraints from $^{40}Ar/^{39}Ar$ dating, elemental and Sr–Nd–Pb isotopic geochemistry of the Mesozoic basalts. Lithos 106, 83–92.
Chen, J.F., Jahn, B.M., 1998. Crustal evolution of southeastern China: Nd and Sr isotopic evidence. Tectonophysics 284, 101–133.
Chen, J.Y., Yang, J.H., Zhang, J.H., Sun, J.F., Wilde, S.A., 2013. Petrogenesis of the Cretaceous Zhangzhou batholith in southeastern China: zircon U–Pb age and Sr–Nd–Hf–O isotopic evidence. Lithos 162–163, 140–156.
Chen, R., Zhou, J.C., 1999. Information of crust–mantle interaction implied in early Cretaceous composite lavas and dikes from eastern Zhejiang. Geol. Rev. 5 (Sup.), 784–795 (in Chinese with English abstract).
Chen, Y.D., Price, R.C., White, A.J.R., Chappell, B.W., 1989. Inclusions in three S-type granites from southeastern Australia. J. Petrol. 30, 1181–1218.
Cheng, Y.B., Spandler, C., Mao, J.W., Rusk, B.G., 2012. Granite, gabbro and mafic microgranular enclaves in the Gejiu area, Yunnan Province, China: a case of twostage mixing of crust- and mantle-derived magmas. Contrib. Miner. Petrol. 164, 659–676.
Clemens, J.D., Wall, V.J., 1988. Controls on the mineralogy of S-type volcanic and plutonic rocks. Lithos 21, 53–66.
Compston, W., Williams, I.S., Kirschvink, J.L., Zhang, Z.C., Ma, G.G., 1992. Zircon U–Pb ages for the Early Cambrian time-scale. J. Geol. Soc. 149, 171–184.
Dahlquist, J.A., 2002. Mafic microgranular enclaves: early segregation from metaluminous magma (Sierra de Chepes), Pampean Ranges, NW Argentina. J. S. Am. Earth Sci. 15 (6), 643–655.

Debon, F., Le Fort, P., 1983. A chemical–mineralogical classification of common plutonic rocks and associations. Trans. R. Soc. Edinburgh: Earth Sci. 73, 135–149.
Donaire, T., Pascual, E., Pin, C., Duthou, J.L., 2005. Microgranular enclaves as evidence of rapid cooling in granitoid rocks: the case of the Los Pedroches granodiorite, Iberian Massif, Spain. Contrib. Miner. Petrol. 149 (3), 247–265.
Dong, C.W., Zhou, X.M., Li, H.M., Ren, S.L., Zhou, X.H., 1997. Late Mesozoic crust–mantle interaction in southeastern Fujian: isotopic evidence from the Pingtan igneous complex. Chin. Sci. Bull. 42, 495–498.
Dong, C.W., Li, W.X., Chen, X.M., Xu, X.S., Zhou, X.M., 1998. Late Mesozoic magma mixing in SE-Fujian: petrologic evidence from Pingtan igneous complex. Prog. Nat. Sci. 8, 196–201.
Dong, C.W., Zhang, D.R., Xu, X.S., Yan, Q., Zhu, G.Q., 2006. SHRIMP U–Pb dating and lithogeochemistry of basic-intermediate dike swarms from Jinjiang, Fujian Province. Acta Petrol. Sin. 22 (6), 1696–1702 (in Chinese with English abstract).
Donskaya, T.V., Gladkochub, D.P., Mazukabzov, A.M., Ivanov, A.V., 2013. Late Paleozoic–Mesozoic subduction-related magmatism at the southern margin of the Siberian continent and the 150 million-year history of the Mongol-Okhotsk Ocean. J. Asian Earth Sci. 62, 79–97.
Dorais, M.J., Whitney, J.A., Roden, M.F., 1990. Origin of mafic enclaves in the Dinkey Creek Pluton, Central Sierra Nevada batholith, California. J. Petrol. 31, 853–881.
Feeley, T.C., Wilson, L.F., Underwood, S.J., 2008. Distribution and compositions magmatic inclusions in the Mount Helen dome, Lassen volcanic center, California: insights into magma chamber processes. Lithos 106, 173–189.
Feldstein, S.N., Lange, R.A., 1999. Pliocene potassic magmas from the Kings River region, Sierra Nevada, California: evidence for melting of a subduction-modified mantle. J. Petrol. 40, 1301–1320.
Feng, S.J., Zhao, K.D., Ling, H.F., Chen, P.R., Chen, W.F., Sun, T., Jiang, S.Y., Pu, W., 2014. Geochronology, elemental and Nd–Hf isotopic geochemistry of Devonian A-type granites in central Jiangxi, South China: Constraints on petrogenesis and post-collisional extension of the Wuyi-Yunkai orogeny. Lithos 206–207, 1–18.
Fernandez, A.N., Barbarin, B., 1991. Relative rheology of coeval mafic and felsic magmas: nature of resulting interaction processes and shape and mineral fabrics of mafic microgranular enclaves. In: Didier, J., Barbarin, B. (Eds.), Enclaves and Granite Petrology. Elsevier, Amsterdam, pp. 263–276.
Ferré, E.C., Caby, R., Peucat, J.J., Capdevila, R., Monié, P., 1998. Pan-African, post-collisional, ferro-potassic granite and quartz–monzonite plutons of Eastern Nigeria. Lithos 45, 255–279.
Frost, B.R., Barnes, C.G., Collins, W.j., Arculus, R.J., Ellis, D.J., Frost, C.D., 2001. A geochemical classification for granitic rocks. J. Petrol. 42 (11), 2033–2048.
Gagnevin, D., Daly, J.S., Poli, G., 2004. Petrographic, geochemical and isotopic constraints on magma dynamics and mixing in the Miocene Monte Capanne monzogranite (Elba Island, Italy). Lithos 78 (1–2), 157–195.
Gao, J.F., Lu, J.J., Lin, Y.P., Pu, W., 2003. Analysis of trace elements in rock samples using HR-ICPMS. J. Nanjing Univ. (Nat. Sci.) 39, 844–850 (in Chinese with English abstract).
Green, T.H., 1995. Significance of Nb/Ta as an indicator of geochemical processes in the crust–mantle system. Chem. Geol. 120, 347–359.
Griffin, W.L., Pearson, N.J., Belousova, E., Jackson, S.E., van Achterbergh, E., O'Reilly, S.Y., Shee, S.R., 2000. The Hf isotope composition of cratonic mantle: LAM-MC-ICPMS analysis of zircon megacrysts in kimberlites. Geochim. Cosmochim. Acta 64 (1), 133–147.
Griffin, W.L., Wang, X., Jackson, S.E., Pearson, N.J., O'Reilly, S.Y., 2002. Zircon geochemistry and magma mixing, SE China: in-situ analysis of Hf isotopes, Tonglu and Pingtan igneous complexes. Lithos 61, 237–269.
Griffin, W.L., Belousova, E.A., Shee, S.R., Pearson, N.J., O'Reilly, S.Y., 2004. Archean crustal evolution in the northern Yilgarn Craton: U–Pb and Hf-isotope evidence from detrital zircons. Precambr. Res. 131, 231–282.
Griffin, W.L., Pearson, N.J., Belousova, E.A., Saeed, A., 2007. Reply to "Comment to short-communication 'Comment: Hf-isotope heterogeneity in zircon 91500' by W.L. Griffin, N.J. Pearson, E.A. Belousova and A. Saeed (Chemical geology 233 (2006) 358-363)" by F. Corfu. Chem. Geol. 244 (1–2), 354–356.
Grogan, S.E., Reavy, R.J., 2002. Disequilibrium textures in the Leinster Granite Complex, SE Ireland: evidence for acid–acid magma mixing. Mineral. Mag. 66 (6), 929–939.
Guo, F., Fan, W.M., Li, C.W., Zhao, L., Li, H.X., Yang, J.H., 2012. Multi-stage crust–mantle interaction in SE China: temporal, thermal and compositional constraints from the Mesozoic felsic volcanic rocks in eastern Guangdong-Fujian provinces. Lithos 150, 62–84.
Hawkesworth, C.J., Kemp, A., 2006. Using hafnium and oxygen isotopes in zircons to unravel the record of crustal evolution. Chem. Geol. 226 (3–4), 144–162.
He, Z.Y., Xu, X.S., Yu, Y., Zou, H.B., 2009. Origin of the Late Cretaceous syenite from Yandangshan, SE China, constrained by zircon U–Pb and Hf isotopes and geochemical data. Int. Geol. Rev. 51 (6), 556–582.
He, Z.Y., Xu, X.S., Niu, Y.L., 2010. Petrogenesis and tectonic significance of a Mesozoic granite–syenite–gabbro association from inland South China. Lithos 119, 621–641.
He, Z.Y., Xu, X.S., 2012. Petrogenesis of the Late Yanshanian mantle-derived intrusions in southeastern China: response to the geodynamics of paleo-Pacific plate subduction. Chem. Geol. 328, 208–221.
Hofmann, A., Jochum, K., Seufert, M., White, M., 1986. Nb and Pb in oceanic basalts: New constraints on mantle evolution. Earth Planet. Sci. Lett. 33, 33–45.
Hofmann, A.W., 1988. Chemical differentiation of the Earth: the relationship between mantle, continental crust, and oceanic crust. Earth Planet. Sci. Lett. 90, 297–314.
Hong, W.T., Xu, X.S., Zou, H.B., 2013. Petrogenesis of coexisting high-silica aluminous and peralkaline rhyolites from Yunshan (Yongtai), southeastern China. J. Asian Earth Sci. 74, 316–329.
Hoskin, P.W.O., Schaltegger, U., 2003. The compositions of zircon and igneous and metamorphic petrogenesis. Rev. Mineral. Geochem. 53, 27–55.
Hsieh, P.S., Chen, C.H., Yang, H.J., Lee, C.Y., 2008. Petrogenesis of the Nanling Mountains granites from South China: constraints from systematic apatite geochemistry and whole-rock geochemical and Sr–Nd isotope compositions. J. Asian Earth Sci. 33, 428–451.
Hsieh, P.S., Chen, C.-H., Yen, C.M., Lee, C.Y., 2009. Origin of mafic microgranular enclaves (MMEs) and their host rocks of the Cretaceous Xiaojiang-Liangnong Granitic Complexes in the Southeast Coast Magmatic Belt, S China. Terrest. Atmos. Oceanic Sci. 20, 481–500.
Ilbeyli, N., Pearce, J.A., 2005. Petrogenesis of igneous enclaves in plutonic rocks of the Central Anatolian Massif, Turkey. Int. Geol. Rev. 47, 1011–1034.
Ionov, D.A., O'Reilly, S.Y., Griffin, W.L., 1997. Volatile-bearing minerals and lithophile trace elements in the upper mantle. Chem. Geol. 141, 153–184.
Irvine, T.N., Baragar, W.R.A., 1971. A guide to the chemical classification of the common volcanic rocks. Can. J. Earth Sci. 8, 523–548.
Jackson, S.E., Pearson, N.J., Griffin, W.L., Belousoval, E.A., 2004. The application of laser ablation-inductively coupled plasma-mass spectrometry (LA-ICP-MS) to in situ U–Pb zircon geochronology. Chem. Geol. 211, 47–69.
Jahn, B.M., Zhou, X.H., Li, J.L., 1990. Formation and tectonic evolution of Southeastern China and Taiwan: isotopic and geochemical constraints. Tectonophysics 183, 145–160.
Jiang, Y.H., Jiang, S.Y., Ling, H.F., Zhou, X.R., Rui, X.J., Yang, W.Z., 2002. Petrology and geochemistry of shoshonitic plutons from the western Kunlun orogenic belt, Xinjiang, northwestern China: implications for granitoid geneses. Lithos 63, 165–187.
Jiang, Y.H., Jin, G.D., Liao, S.Y., Zhou, Q., Zhao, P., 2012. Petrogenesis and tectonic implications of ultrapotassic microgranitoid enclaves in Late Triassic arc granitoids, Qinling orogen, central China. Int. Geol. Rev. 54 (2), 208–226.
Jiang, Y.H., Jia, R.Y., Liu, Z., Liao, S.Y., Zhao, P., Zhou, Q., 2013. Origin of Middle Triassic high-K calc-alkaline granitoids and their potassic microgranular enclaves from the western Kunlun orogen, northwest China: a record of the closure of Paleo-Tethys. Lithos 156–159, 13–30.
Kadioglu, Y.K., Gulec, N., 1999. Types and genesis of the enclaves in central Anatolian granitoids. Geol. J. 34, 243–256.
Kamber, B.S., Collerson, K.D., 2000. Role of 'hidden' deeply subducted slabs in mantle depletion. Chem. Geol. 166, 241–254.
Kaygusuz, A., Arslan, M., Siebel, W., Sipahi, F., İlbeyli, N., Temizel, İ., 2014. LA-ICP MS zircon dating, whole-rock and Sr–Nd–Pb–O isotope geochemistry of the Camiboğazı pluton, Eastern Pontides, NE Turkey: implications for lithospheric mantle and lower crustal sources in arc-related I-type magmatism. Lithos 192–195, 271–290.
Klemme, S., Prowatke, S., Hametner, K., Gunther, D., 2005. Partitioning of trace elements between rutile and silicate melts: implications for subduction zones. Geochim. Cosmochim. Acta 69, 2361–2371.
Kocak, K., 2006. Hybridization of mafic microgranular enclaves: mineral and whole-rock chemistry evidence from the Karamadazi Granitoid, Central Turkey. Int. J. Earth Sci. 95, 587–607.
Kocak, K., Zedef, V., Kansun, G., 2011. Magma mixing/mingling in the Eocene Horoz (Nigde) granitoids, Central southern Turkey: evidence from mafic microgranular enclaves. Mineral. Petrol. 103 (1–4), 149–167.
Kumar, S., Rino, V., Pal, A.B., 2004. Field evidence of magma mixing from microgranular enclaves hosted in Palaeoproterozoic Malanjkhand granitoids, Central India. Gondwana Res. 7 (2), 539–548.
Kumar, K.V., Frost, C.D., Frost, B.R., Chamberlain, K.R., 2007. The Chimakurti, Errakonda, and Uppalapadu plutons, Eastern Ghats Belt, India: an unusual association of tholeiitic and alkaline magmatism. Lithos, 30–57.
Köksal, S., Toksoy-Köksal, F., Göncüoğlu, M.C., Möller, A., Gerdes, A., Frei, D., 2013. Crustal source of the Late Cretaceous Satansarı monzonite stock (central Anatolia–Turkey) and its significance for the Alpine geodynamic evolution. J. Geodyn. 65, 82–93.
Lan, T.G., Fan, H.R., Hu, F.F., Tomkins, A.G., Yang, K.F., Liu, Y.S., 2011. Multiple crust–mantle interactions for the destruction of the North China Craton: geochemical and Sr–Nd–Pb–Hf isotopic evidence from the Longbaoshan alkaline complex. Lithos 122, 87–106.
Lan, T.G., Fan, H.R., Santosh, M., Hu, F.F., Yang, K.F., Yang, Y.H., Liu, Y.S., 2012. Early Jurassic high-K calc-alkaline and shoshonitic rocks from the Tongshi intrusive complex, eastern North China Craton: implication for crust–mantle interaction and post-collisional magmatism. Lithos 140–141, 183–199.
Lan, T.G., Fan, H.R., Santosh, M., Hu, F.F., Yang, K.F., Yang, Y.H., Yang, Y.H., Liu, Y.S., 2013. Crust–mantle interaction beneath the Luxi Block, eastern North China Craton: evidence from coexisting mantle- and crust-derived enclaves in a quartz monzonite pluton. Lithos 177, 1–6.
Li, B., Jiang, S.Y., 2014a. A subduction-related metasomatically enriched mantle origin for the Luoboling and Zhongliao Cretaceous granitoids from South China: implications for magma evolution and Cu–Mo mineralization. Int. Geol. Rev. http://dx.doi.org/10.1080/00206814.2014.979452.
Li, B., Jiang, S.Y., 2014b. Geochronology and geochemistry of Cretaceous Nanshanping alkaline rocks from the Zijinshan district in Fujian Province, South China: implications for crust–mantle interaction and lithospheric extension. J. Asian Earth Sci. 93, 253–274.
Li, C., van der Hilst, R.D., 2010. Structure of the upper mantle and transition zone beneath Southeast Asia from traveltime tomography. J. Geophys. Res. 115, B07308. http://dx.doi.org/10.1029/2009JB006882.
Li, J.X., Qin, K.Z., Li, G.M., Richards, J.P., Zhao, J.X., Cao, M.J., 2014. Geochronology, geochemistry, and zircon Hf isotopic compositions of Mesozoic intermediate–felsic intrusions in central Tibet: petrogenetic and tectonic implications. Lithos 198–199, 77–91.

Li, X.H., Hu, R.Z., Rao, B., 1997. Geochronology and geochemistry of Cretaceousmafic dikes from northern Guangdong, SE China. Geochimica 26, 14–31 (in Chinese with English abstract).
Li, X.H., 2000. Cretaceous magmatism and lithospheric extension in Southeast China. J. Asian Earth Sci. 18 (3), 293–305.
Li, X.H., Chung, S.L., Zhou, H.W., Lo, C.H., Liu, Y., Chen, C.H., 2004. Jurassic intraplate magmatism in southern Hunan-eastern Guangxi: $^{40}Ar/^{39}Ar$ dating, geochemistry, Sr–Nd isotopes and implications for tectonic evolution of SE China. In: Malpas, J., Fletcher, C.J., Aitchison, J.C., et al. (Eds.), Aspects of the Tectonic Evolution of China. Geological Society, London, Special Publications, 226, pp. 193–216.
Li, X.H., Li, Z.X., Li, W.X., Liu, Y., Yuan, C., Wei, G.J., Qi, C.S., 2007. U–Pb zircon, geochemical and Sr–Nd–Hf isotopic constraints on age and origin of Jurassic I- and A-type granites from central Guangdong, SE China: a major igneous event in response to foundering of a subducted flat-slab? Lithos 96 (1–2), 186–204.
Li, X.H., Li, W.X., Li, Z.X., Lo, C.H., Wang, J., Ye, M.F., Yang, Y.H., 2009. Amalgamation between the Yangtze and Cathaysia Blocks in South China: constraints from SHRIMP U–Pb zircon ages, geochemistry and Nd–Hf isotopes of the Shuangxiwu volcanic rocks. Precambr. Res. 174, 117–128.
Li, X.H., Li, Z.X., He, B., Li, W.X., Li, Q.L., Gao, Y.Y., Wang, X.C., 2012. The Early Permian active continental margin and crustal growth of the Cathaysia Block: in situ U–Pb, Lu–Hf and O isotope analyses of detrital zircons. Chem. Geol. 328, 195–207.
Li, Z.X., Li, X.H., 2007. Formation of the 1300-km-wide intracontinental orogen and postorogenic magmatic province in Mesozoic South China: a flat-slab subduction model. Geology 35, 179–182.
Li, Z., Qiu, J.S., Xu, X.S., 2012. Geochronological, geochemical and Sr–Nd–Hf isotopic constraints on petrogenesis of Late Mesozoic gabbro-granite complexes on the southeast coast of Fujian, South China: insights into a depleted mantle source region and crust–mantle interactions. Geol. Mag. 149 (3), 459–482.
Li, Z., Qiu, J.S., Yang, X.M., 2014. A review of the geochronology and geochemistry of Late Yanshanian (Cretaceous) plutons along the Fujian coastal area of southeastern China: implications for magma evolution related to slab breakoff and rollback in the Cretaceous. Earth Sci. Rev. 128, 232–248.
Li, Z.X., Wartho, J.A., Occhipinti, S., Zhang, C.L., Li, X.H., Wang, J., Bao, C., 2007. Early history of the eastern Sibao orogen (South China) during the assembly of Rodinia: new mica 40Ar/39Ar dating and SHRIMP U–Pb detrital zircon provenance constraints. Precambr. Res. 159, 79–94.
Ling, M.X., Wang, F.Y., Ding, X., Hu, Y.H., Zhou, J.B., Zartman, R.E., Yang, X.Y., Sun, W. D., 2009. Cretaceous ridge subduction along the Lower Yangtze River Belt, eastern China. Econ. Geol. 104, 303–321.
Liu, L., Xu, X.S., Zou, H.B., 2012. Episodic eruptions of the Late Mesozoic volcanic sequences in southeastern Zhejiang, SE China: petrogenesis and implications for the geodynamics of paleo-Pacific subduction. Lithos 154, 166–180.
Liu, L., Xu, X.S., Xia, Y., 2014a. Cretaceous Pacific plate movement beneath SE China: evidence from episodic volcanism and related intrusions. Tectonophysics 614, 170–184.
Liu, L., Qiu, J.S., Li, Z., 2013. Origin of mafic microgranular enclaves (MMEs) and their host quartz monzonites from the Muchen pluton in Zhejiang Province, Southeast China: Implications for magma mixing and crust–mantle interaction. Lithos 160–161, 145–163.
Liu, L., Qiu, J.S., Zhao, J.L., Yang, Z.L., 2014b. Geochronological, geochemical, and Sr–Nd–Hf isotopic characteristics of Cretaceous monzonitic plutons in western Zhejiang Province, Southeast China: new insights into the petrogenesis of intermediate rocks. Lithos 196–197, 242–260.
Liu, Q., Yu, J.H., Wang, Q., Su, B., Zhou, M.F., Xu, H., Cui, X., 2012. Ages and geochemistry of granites in the Pingtan-Dongshan Metamorphic Belt, Coastal South China: new constraints on Late Mesozoic magmatic evolution. Lithos 150, 268–286.
Liu, S., Hu, R.Z., Gao, S., Feng, C., Qi, Y.Q., Wang, T., Feng, G.Y., Coulson, I.M., 2008. U–Pb zircon age, geochemical and Sr–Nd–Pb–Hf isotopic constraints on age and origin of alkaline intrusions and associated mafic dikes from Sulu orogenic belt, Eastern China. Lithos 106, 365–379.
Lloyd, F.E., Arima, M., Edgar, A.D., 1985. Partial melting of a phlogopite–clinopyroxenite nodule from southwest Uganda: an experimental study bearing on the origin of highly potassic continental rift volcanics. Contrib. Miner. Petrol. 91, 321–329.
Lowell, G.R., Young, G.J., 1999. Interaction between coeval mafic and felsic melts in the St. Francois Terrane of Missouri, USA. Precambr. Res. 95 (1–2), 69–88.
Ludwig, K.R., 2001. Isoplot/Ex (rev. 2.49): A Geochronological Toolkit for Microsoft Excel. Berkeley Geochronology Center, Special Publication, No. 1, pp. 1–58.
Ma, L., Jiang, S.Y., Hou, L.M., Dai, B.Z., Jiang, Y.H., Yang, T., Zhao, K.D., Pu, W., Zhu, Z.Y., Xu, B., 2014. Geochemistry of Early Cretaceous calc-alkaline lamprophyres in the Jiaodong Peninsula: implication for lithospheric evolution of the eastern North China Craton. Gondwana Res. 25 (2), 859–872.
Maniar, P.D., Piccoli, P.M., 1989. Tectonic discrimination of granitoids. Geol. Soc. Am. Bull. 101, 635–643.
Mao, J.R., Ye, H.M., Liu, K., Li, Z.L., Takahashi, Y., Zhao, X.L., Kee, Weon.-Seo., 2013. The Indosinian collision–extension event between the South China Block and the Palaeo-Pacific plate: evidence from Indosinian alkaline granitic rocks in Dashuang, eastern Zhejiang, South China. Lithos 172–173, 81–97.
McDonough, W.F., Sun, S.S., 1995. The composition of the Earth. Chem. Geol. 120, 223–253.
Meng, L.F., Li, Z.X., Chen, H.L., Li, X.H., Wang, X.C., 2012. Geochronological and geochemical results from Mesozoic basalts in southern South China Block support the flat-slab subduction model. Lithos 132–133, 127–140.
Middlemost, E.A.K., 1985. Magma and Magmatic Rocks. Longman, London.
Middlemost, E.A.K., 1994. Naming materials in the magma/igneous rock system. Earth Sci. Rev. 37, 215–224.
Miller, R.G., O'Nions, R.K., 1985. Source of Precambrian chemical and clastic sediments. Nature 314, 325–330.
Neves, S.P., Mariano, G., 1997. High-K calc-Alkalic plutons in Northeast Brazil: origin of the biotite diorite/quartz monzonite to granite association and implications for the evolution of the Borborema Province. Int. Geol. Rev. 39 (7), 621–638.
Noyes, H.J., Frey, F.A., Wones, D.R., 1983. A tale of two plutons: geochemical evidence bearing on the origin and differentiation of the Red Lake and Eagle Peak plutons, Central Sierra Nevada, California. J. Geol. 91, 487–509.
Orsini, J.B., Cocirta, C., Zorpi, M.J., 1991. Genesis of mafic microgranular enclaves through differentiation of basic magmas, mingling and chemical exchanges with their host granitoid magmas. In: Didier, J., Barbarin, B. (Eds.), Enclaves and Granite Petrology, Developments in Petrology. Elsevier Science Ltd, Amsterdam, pp. 445–464.
Pagel, M., Leterrier, J., 1980. The subalkaline potassic magmatism of the Ballons massif (Southern Vosges, France): shoshonitic affinity. Lithos 13, 1–10.
Patiño Douce, A.E., Johnston, A.D., 1991. Phase equilibria and melt productivity in the pelitic system: implications for the origin of peraluminous granitoids and aluminous granulites. Contrib. Miner. Petrol. 107, 202–218.
Pearce, J.A., 1996. Sources and settings of granitic rocks. Episodes 19, 120–125.
Pearce, J.A., Harris, N.B.W., Tindle, A.G., 1984. Trace element discrimination diagrams for the tectonic interpretation of granitic rocks. J. Petrol. 25, 956–983.
Peccerillo, A., Taylor, D.R., 1976. Geochemistry of Eocene calc-alkaline volcanic rocks from the Kaitamonu area, Northern Turkey. Contrib. Miner. Petrol. 58, 63–91.
Perugini, D., Poli, G., Christofides, G., Eleftheriadis, G., 2003. Magma mixing in the Sithonia plutonic complex, Greece: evidence from mafic microgranular enclaves. Mineral. Petrol. 78, 173–200.
Pu, W., Zhao, K.D., Ling, H.F., Jiang, S.Y., 2004. High precision Nd isotope measurement by Triton TI Mass Spectrometry. Acta Geosci. Sin. 25, 271–274 (in Chinese with English abstract).
Pu, W., Gao, J.F., Zhao, K.D., Lin, H.F., Jiang, S.Y., 2005. Separation method of Rb–Sr, Sm,–Nd using DCTA and HIBA. J. Nanjing Univ. (Nat. Sci.) 41, 445–450 (in Chinese with English abstract).
Pupin, J.P., 1980. Zircon and granite petrology. Contrib. Mineral. Petrol. 73, 207–220.
Qiu, J.S., Wang, D.Z., Mcinnes, B.I.A., 1999. Geochemistry and petrogenesis of the I- and A-type composite granite masses in the coastal area of Zhejiang and Fujian province. Acta Petrol. Sin. 15, 237–246 (in Chinese).
Qiu, J.S., Wang, D.Z., Brent, I.A.M., Jiang, S.Y., Wang, R.C., Kanisawa, S., 2004. Two subgroups of A-type granites in the coastal area of Zhejiang and Fujian Provinces, SE China: age and geochemical constraints on their petrogenesis. Trans. R. Soc. Edinburgh: Earth Sci. 95, 227–236.
Qiu, J.S., Xiao, E., Hu, J., Xu, X.S., Jiang, S.Y., Li, Z., 2008. Petrogenesis of highly fractionated Itype granites in the coastal area of northeastern Fujian Province: constraints from zircon U–Pb geochronology, geochemistry and Nd–Hf isotopes. Acta Petrol. Sin. 24, 2468–2484 (in Chinese with English abstract).
Qiu, J.S., Li, Z., Liu, L., Zhao, J.L., 2012. Petrogenesis of the Zhangpu composite granite pluton in Fujian Province: constraints from zircon U–Pb ages, elemental geochemistry and Nd–Hf isotopes. Acta Geol. Sin. 4, 561–576 (in Chinese with English abstract).
Rapela, C.W., Pankhurst, R.J., 1996. Monzonite suites: the innermost Cordilleran plutonism of Patagonia. Trans. R. Soc. Edinburgh: Earth Sci. 87, 193–203.
Rapp, R.P., Watson, E.B., 1995. Dehydration melting of metabasalt at 8–32 kbar: implications for continental growth and crust–mantle recycling. J. Petrol. 36, 891–931.
Rudnick, R.L., Fountain, D.M., 1995. Nature and composition of the continental crust: a lower crustal perspective. Rev. Geophys. 33 (3), 267–309.
Rudnick, R.L., Gao, S., 2003. Composition of the continental crust. In: Holland, H.D., Turekian, K.K. (Eds.), The Crust. Treatise on Geochemistry, 3. Elsevier-Pergamon, Oxford, pp. 1–64.
Ryerson, F.J., Watson, E.B., 1987. Rutile saturation in magmas: implications for Ti–Nb–Ta depletion in island-arc basalts. Earth Planet. Sci. Lett. 86, 225–239.
Shellnutt, J.G., Jahn, B.M., Dostal, J., 2010. Elemental and Sr–Nd isotope geochemistry of microgranular enclaves from peralkaline A-type granitic plutons of the Emeishan large igneous province, SW China. Lithos 119 (1–2), 34–46.
Shu, L., Faure, M., Wang, B., Zhou, X., Song, B., 2008. Late Palaeozoic–Early Mesozoic geological features of South China: response to the Indosinian collision events in Southeast Asia. C.R. Geosci. 340, 151–165.
Sisson, T.W., Ratajeski, K., Hankins, W.B., Glazner, A.F., 2005. Voluminous granitic magmas from common basaltic sources. Contrib. Miner. Petrol. 148, 635–661.
Sparks, R.S.J., Sigurdsson, H., Wilson, L., 1977. Magma mixing: a mechanism for triggering acid explosive eruptions. Nature 267, 315–317.
Sparks, R.S.J., Marshall, L., 1986. Thermal and mechanical constraints on mixing between mafic and silicic magmas. J. Volcanol. Geoth. Res. 29, 99–124.
Stern, R.J., 2002. Subduction zones. Rev. Geophys. 40 (4), 1012–1049.
Sun, S.S., McDonough, W.F., 1989. Chemical and isotopic systematics of oceanic basalts: implications for mantle composition and processes. In: Saunders, A.D., Norry, M.J. (Eds.), Magmatism in the Ocean Basins, Geological Society of London Special Publication, pp. 313–345.
Sun, W.D., Ding, X., Hu, Y.H., Li, X.H., 2007. The golden transformation of the Cretaceous plate subduction in the west Pacific. Earth Planet. Sci. Lett. 262, 533–542.
Tao, K.Y., Xing, G.F., Yang, Z.L., Mao, J.R., Zhao, Y., Xu, N.Z., et al., 2000. Determination of and discussion on the ages of Mesozoic volcanic rocks in Zhejiang: comment

on the argumentation of Lapierre et al. Geol. Rev. 46, 14–21 (in Chinese with English abstract).
Taylor, S.R., McLennan, S.M., 1985. The Continental Crust: Its Composition and Evolution. Blackwell Press, Oxford, p. 312.
Van Achterbergh, E., Ryan, C.G., Jackson, S.E., Griffin, W.L., 2001. Data reduction software for La-ICP-MS: appendix. In: Sylvester, P.J. (Ed.), Laser Ablation-ICP-Mass-Spectrometry in the Earth Sciences: Principles and Applications. Mineralogist Association Canada Short Course Series, Ottawa, pp. 239–243.
Vernon, R.H., 1984. Microgranitoid enclaves in granites: globules of hybrid magma quenched in a plutonic environment. Nature 309 (5967), 438–439.
Vernon, R.H., Etheridge, M.A., Wall, V.J., 1988. Shape and microstructure of microgranitoid enclaves: indicators of magma mingling and flow. Lithos 22 (1), 1–11.
Wang, D.X., Li, C.L., Gao, W.L., Wang, Z.X., Zhao, Z.D., 2013. Late Mesozoic magma mixing in eastern Zhejiang Province: evidence from U–Pb geochronology and geochemistry of Xiaojiang pluton in Xinchang. Acta Petrol. Sin. 29 (11), 3993–4003 (in Chinese with English abstract).
Wang, D.Z., Zhou, J.C., 2005. New progress in studying the Large Igneous Provinces. Geol. J. China Univ. 11 (1), 1–8 (in Chinese with English abstract).
Wang, F., Lu, X.X., Lo, C.H., Wu, F.Y., He, Y.H., Yang, L.K., Zhu, R.X., 2007. Post-collisional, potassic monzonite–minette complex (Shahewan) in the Qinling Mountains (central China): 40Ar/39Ar thermochronology, petrogenesis, and implications for the dynamic setting of the Qinling orogen. J. Asian Earth Sci. 31, 153–166.
Wang, F.Y., Ling, M.X., Ding, X., Hu, Y.H., Zhou, J.B., Yang, X.Y., Liang, H.Y., Fan, W.M., Sun, W.D., 2011. Mesozoic large magmatic events and mineralization in SE China: oblique subduction of the Pacific plate. Int. Geol. Rev. 53, 704–726.
Wang, Q., Li, J.W., Jian, P., Zhao, Z.H., Xiong, X.L., Bao, Z.W., Xu, J.F., Li, C.F., Ma, J.L., 2005. Alkaline syenites in eastern Cathaysia (South China): link to Permian–Triassic transtension. Earth Planet. Sci. Lett. 230, 339–354.
Wang, W., Liu, S.W., Bai, X., Li, Q.G., Yang, P.T., Zhao, Y., 2013. Geochemistry and zircon U–Pb–Hf isotopes of the late Paleoproterozoic Jianping diorite–monzonite–syenite suite of the North China Craton: implications for petrogenesis and geodynamic setting. Lithos 162–163, 175–194.
Wang, X., 1998. Quantitative description of zircon morphology and its dynamics analysis. Sci. China, Ser. D: Earth Sci. 41, 422–428.
Wang, X., Kienast, J.R., 1999. Morphology and geochemistry of zircon: a case study on zircon from the microgranitoid enclaves. Sci. China, Ser. D: Earth Sci. 42, 544–552.
Wang, Y.J., Fan, W.M., Peter, A., Cawood, Li.S.Z., 2008. Sr–Nd–Pb isotopic constraints on multiple mantle domains for Mesozoic mafic rocks beneath the South China Block. Lithos 106, 297–308.
Wang, Z.H., 2002. The origin of the Cretaceous gabbros in the Fujian coastal region of SE China: implications for deformation-accompanied magmatism. Contrib. Miner. Petrol. 144, 230–240.
Watson, E.B., Harrison, T.M., 1983. Zircon saturation revisited: temperature and composition effects in a variety of crustal magma types. Earth Planet. Sci. Lett. 64, 295–304.
Whalen, J.B., Currie, K.L., Chappell, B.W., 1987. A-type granites: geochemical characteristics, discrimination and petrogenesis. Contrib. Mineral. Petrol. 95, 407–419.
Wiebe, R.A., 1973. Relations between coexisting basaltic and granitic magmas in a composite dike. Am. J. Sci. 273, 130–151.
Wiebe, R.A., Smith, D., Sturn, M., King, E.M., 1997. Enclaves in the Cadillac mountain granite (Coastal Maine): samples of hybrid magma from the base of the chamber. J. Petrol. 38, 393–426.
White, R.V., Tarney, J., Kerr, A.C., Saunders, A.D., Kempton, P.D., Pringle, M.S., Klaver, G.T., 1999. Modification of an oceanic plateau, Aruba, Dutch Caribbean: implications for the generation of continental crust. Lithos 46, 43–68.
Wong, J., Sun, M., Xing, G.F., Li, X.H., Zhao, G.C., Wong, K., Yuan, C., Xia, X.P., Li, L.M., Wu, F.Y., 2009. Geochemical and zircon U–Pb and Hf isotopic study of the Baijuhuajian metaluminous A-type granites: extension at 125–100 Ma and its tectonic significance for South China. Lithos 112, 289–305.
Wu, C.L., Dong, S.W., Robinson, P.T., Frost, B.R., Gao, Y.H., Lei, M., Chen, Q.L., Qin, H.P., 2014. Petrogenesis of high-K, calc-alkaline and shoshonitic intrusive rocks in the Tongling area, Anhui Province (eastern China), and their tectonic implications. Geol. Soc. Am. Bull. 126, 78–102.
Wu, F.Y., Jahn, B.M., Wilde, S.A., Lo, C.H., Yui, T.F., Lin, Q., Ge, W.C., Sun, D.Y., 2003. Highly fractionated I-type granites in NE China (II): isotopic geochemistry and implications for crustal growth in the Phanerozoic. Lithos 67, 191–204.
Wu, Y.B., Zheng, Y.F., 2004. Genesis of zircon and its constraints on interpretation of U–Pb age. Chin. Sci. Bull. 49 (15), 1554–1569.
Xie, L., Wang, D.Z., Wang, R.C., Qiu, J.S., Chen, X.M., 2004. Complex zoning texture in plagiochases from the quartz diorite enclave in the Putuo granitic complex, Zhejiang Province: record of magma mixing. Acta Petrol. Sin. 20 (6), 1397–1408 (in Chinese with English abstract).
Xing, G.F., Chen, R., Yang, Z.L., Zhou, Y.Z., Li, L.M., Jiang, Y., Chen, Z.H., 2009. Characteristics and tectonic setting of Late Cretaceous volcanic magmatism in the coastal Southeastern China. Acta Petrol. Sin. 25, 77–91 (in Chinese with English abstract).
Xiong, F.H., Ma, C.Q., Zhang, J.Y., Liu, B., 2011. The origin of mafic microgranular enclaves and their host granodiorites from East Kunlun, Northern Qinghai-Tibet Plateau: implications for magma mixing during subduction of Paleo-Tethyan lithosphere. Mineral. Petrol. 104, 211–224.
Xu, X.S., O'Reilly, S.Y., Zhou, X.M., Griffin, W.L., 1996. A xenolith-derived geotherm and the crust–mantle boundary at Qilin, southeastern China. Lithos 38, 41–62.
Xu, X.S., Dong, C.W., Li, W.X., Zhou, X.M., 1999. Late Mesozoic intrusive complexes in the coastal area of Fujian, SE China: the significance of the gabbro-diorite-granite association. Lithos 46, 299–315.
Xu, X.S., O'reilly, S.Y., Griffin, W.L., Zhou, X.M., 2000. Genesis of young lithospheric mantle in Southeastern China: an LAM-ICPMS trace element study. J. Petrol. 41, 111–148.
Xu, X.S., O'Reilly, S.Y., Griffin, W.L., Wang, X.L., Pearson, N.J., He, Z.Y., 2007. The Crust of Cathaysia: age, assembly and reworking of two Terranes. Precambr. Res. 158, 51–78.
Xu, Y.G., Huang, X.L., Ma, J.L., Wang, Y.B., Iizuka, Y., Xu, J.F., Wang, Q., Wu, X.Y., 2004. Crust–mantle interaction during the tectono-thermal reactivation of the North China Craton: constraints from SHRIMP zircon U–Pb chronology and geochemistry of Mesozoic plutons from western Shandong. Contrib. Miner. Petrol. 147, 750–767.
Xu, Y.G., Ma, J.L., Frey, F.A., Feigenson, M.D., Liu, J.F., 2005. Role of lithosphere–asthenosphere interaction in the genesis of Quaternary alkali and tholeiitic basalts from Datong, western North China Craton. Chem. Geol. 224, 247–271.
Xue, H.M., Tao, K.Y., Shen, J.L., 1996. Sr and Nd isotopic characteristics and magma genesis of Mesozoic volcanic rocks along the coastal region of Southeastern China. Acta Petrol. Sin. 9, 260–273 (in Chinese with English abstract).
Yaliniz, M.K., Aydin, N.S., Göncüoglu, M.C., Parlak, O., 1999. Terlemez quartz monzonite of central Anatolia (Aksaray-Sarkaraman): age, petrogenesis, and geotectonic implications for ophiolite emplacement. Geol. J. 34, 233–242.
Yang, J.H., Wu, F.Y., Chung, S.L., Wilde, S.A., Chu, M.F., 2006. A hybrid origin for the Qianshan A-type granite, northeast china: geochemical and Sr–Nd–Hf isotopic evidence. Lithos 89 (1–2), 89–106.
Yang, J.H., Wu, F.Y., Wilde, S.A., Xie, L.W., Yang, Y.H., Liu, X.M., 2007. Trace magma mixing in granite genesis: in-situ U–Pb dating and Hf-isotope analysis of zircons. Contrib. Mineral. Petrol. 153, 177–190.
Yang, S.Y., Jiang, S.Y., Jiang, Y.H., Zhao, K.D., Fan, H.H., 2011. Geochemical, zircon U–Pb dating and Sr–Nd–Hf isotopic constraints on the age and petrogenesis of an Early Cretaceous volcanic-intrusive complex at Xiangshan, Southeast China. Mineral. Petrol. 101, 21–48.
Ye, M.F., Li, X.H., Li, W.X., Liu, Y., Li, Z.X., 2007. SHRIMP zircon U–Pb geochronological and whole-rock geochemical evidence for an early Neoproterozoic Sibaoan magmatic arc along the southeastern margin of the Yangtze Block. Gondwana Res. 12, 144–156.
Yu, J.H., O'Reilly, S.Y., Suzanne, Y., Wang, L.J., Griffin, W.L., Zhou, M.F., Zhang, M., Shu, L.S., 2010. Components and episodic growth of Precambrian crust in the Cathaysia Block, South China: evidence from U–Pb ages and Hf isotopes of zircons in Neoproterozoic sediments. Precambr. Res. 181 (1–4), 97–114.
Zhang, X.L., Qiu, J.S., Wang, D.Z., Wang, R.C., Xu, X.S., Chen, X.M., 2005. Geochemistry and magmatic mixing of the Putuoshan biotite moyites and their enclaves, Zhejiang Province. Acta Petrol. Mineral. 24 (2), 81–92 (in Chinese with English abstract).
Zhang, Z.J., Badal, B., Li, Y.K., Chen, Y., Yang, L.P., Teng, J.W., 2005. Crust–uppermantleseismic velocity structure across Southeastern China. Tectonophysics 395, 137–157.
Zhang, Z.J., Wang, Y.H., 2007. Crustal structure and contact relationship revealed from deep seismic sounding data in South China. Phys. Earth Planet. Inter. 165, 114–126.
Zhang, Z.J., Zhang, X., Badal, J., 2008. Composition of the crust beneath southeastern China derived from an integrated geophysical data set. J. Geophys. Res. 113, B04417. http://dx.doi.org/10.1029/2006JB004503.
Zhao, J.L., Qiu, J.S., Liu, L., Wang, R.Q., 2015. Geochronological, geochemical and Nd–Hf isotopic constraints on the petrogenesis of Late Cretaceous A-type granites from the southeastern coast of Fujian Province, South China. J. Asian Earth Sci. 105, 338–359.
Zhao, K.D., Jiang, S.Y., Yang, S.Y., Dai, B.Z., Lu, J.J., 2012. Mineral chemistry, trace elements and Sr–Nd–Hf isotope geochemistry and petrogenesis of Cailing and Furong granites and mafic enclaves from the Qitianling batholith in the Shi-Hang zone, South China. Gondwana Res. 22, 310–324.
Zheng, Y.F., Xiao, W.J., Zhao, G.C., 2013. Introduction to tectonics of China. Gondwana Res. 23, 1189–1206.
Zhou, X.M., Li, W.X., 2000. Origin of Late Mesozoic igneous rocks in Southeastern China: implications for lithosphere subduction and underplating of mafic magmas. Tectonophysics 326, 269–287.
Zhou, X.M., Sun, T., Shen, W.Z., Shu, L.S., Niu, Y.L., 2006. Petrogenesis of Mesozoic granitoids and volcanic rocks in South China: a response to tectonic evolution. Episodes 29, 26–33.

Further reading

Soderlund, U., Patchett, P.J., Vervoort, J.D., Isachsen, C.E., 2004. The 176Lu decay constant determined by Lu/Hf and U/Pb isotope systematics of Precambrian mafic intrusions. Earth Planet. Sci. Lett. 219, 311–324.
Vervoort, J.D., Blichert-Toft, J., 1999. Evolution of the depleted mantle: Hf isotope evidence from juvenile rocks through time. Geochim. Cosmochim. Acta 63, 533–556.